Particle Colliders and the LHC

Ewen H. Maclean

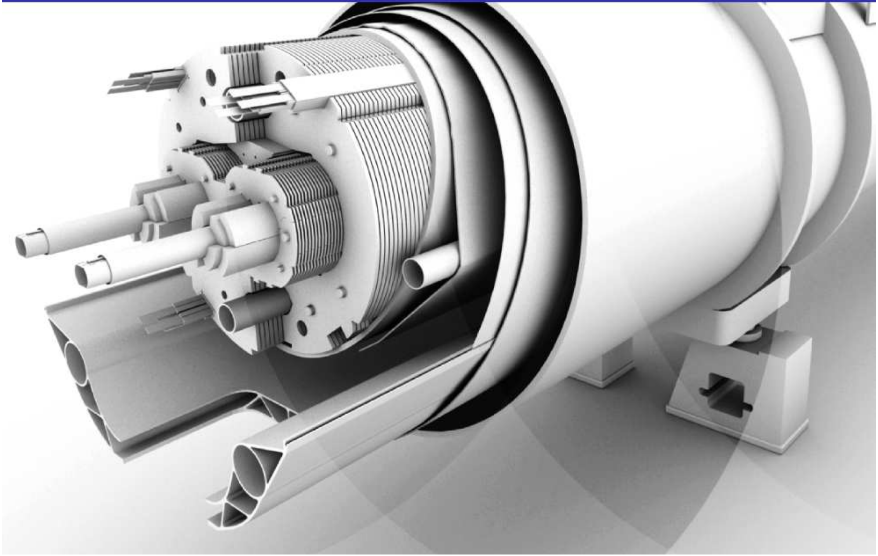

symmetry topics follow +

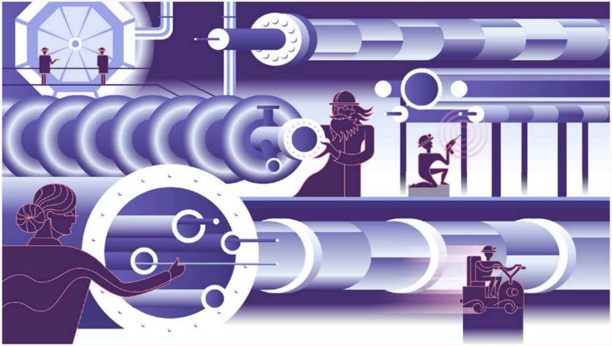

Artwork by Sandbox Studio, Chicago with Ana Kova

The hottest job in physics?

04/26/16 | By Troy Rummler

Accelerator scientists are in demand at labs and beyond.

While the supply of accelerator physicists in the United States has grown modestly over the last decade, it hasn't been able to catch up with demand fueled by industry interest in medical particle accelerators and growing collaborations at the national labs.

~35,000 particle accelerators world-wide

Medicine

physicsworld | Magazine | Latest | People | Impact |

particle therapy

PARTICLE THERAPY | ANALYSIS

Proton therapy on an upward trajectory

16 Feb 2019

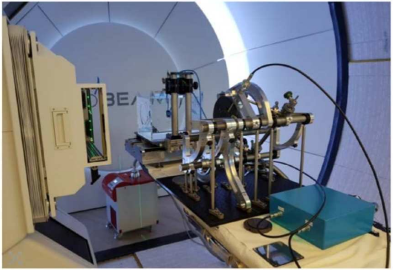

Setting the standard: NPL's portable calorimeter provides a more accurate reference point for proton-beam dosimetry. (Courtesy: NPL)

BBC Sign in | News | Sport | Weather | Shop | Reel | Travel

NEWS

Home | Video | World | UK | Business | Tech | Science | Stories | Entertainment & Arts

Wales | Wales Politics | Wales Business | North West | North East | Mid | South West

Wales cancer patients to get proton beam therapy on NHS

12 December 2018

Share

The centre in Newport will be the second in the UK to offer proton beam therapy on the NHS

Industry & energy

Science & Technology Facilities Council | UK Research and Innovation

Funding | Research | Innovation | Skills | Public engagement | News, events and publications | Abou

Home / News / STFC launches VELA – bringing a new imaging capability for UK industry

STFC launches VELA – bringing a new imaging capability for UK industry

13 March 2015

CERNCOURIER Reporting on international high-energy physics

Physics | Technology | Community | In focus | Magazine

NEWS

GUINEVERE: towards cleaner nuclear energy

27 March 2012

The accelerator used to produce fast neutrons.
Image credit: SCK•CEN. Used by permission.

A particle accelerator has been successfully coupled to a nuclear reactor for the first time at the Belgian Nuclear Research Centre (SCK•CEN). The demonstration model GUINEVERE is now in operation, showing the feasibility of an accelerator-driven system (ADS) for nuclear energy (Mumbai engages ADS for nuclear energy). By using an ADS, the accelerator can be turned off to stop the reactor immediately. This system, known as subcritical, is safer than standard nuclear reactors.

GUINEVERE is a test installation of limited power to fine-tune the operation and control of future subcritical reactors. Unlike conventional reactor systems, it produces fast neutrons that can be used for the transmutation of high-level radioactive waste into less-toxic products with shorter life spans, helping to improve their geological disposal.

Light Sources

Facilitate many types of research:

- Life science
- Chemistry
- Engineering
- Earth science
- Environmental science
- Life science
- Physics/material science
- Cultural heritage
- Forensics
- Food science
- Oceanography
- …

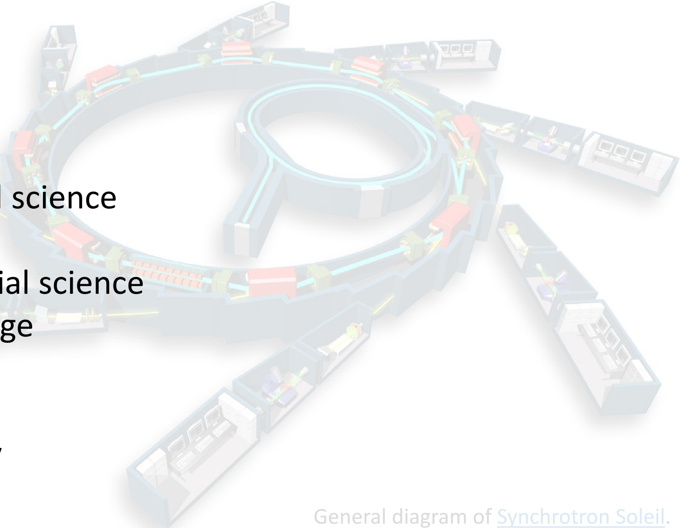

General diagram of Synchrotron Soleil.

Light Sources

Facilitate many types of research:

- Life science

https://www.helmholtz-berlin.de/forschung/unsere-forschung/photonenforschung/corona-forschung_en.html

Research on SARS-CoV-2 at BESSY II

At synchrotron light sources like BESSY II, research is currently gaining crucial insights into combating the SARS-CoV2 virus. The results are helping to contain the spread and fight the disease more effectively.

For corona research, BESSY II has provided access via a fast-track method even during the strictest lockdown phases. Immediately after the genome of the novel coronavirus SARS-CoV2 was sequenced in early 2020, the first measurements of viral proteins started at BESSY II.

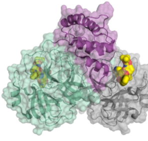

Schematic picture of the coronavirus protease.
(© H. Tabermann / HZB)

- **A first major success at the beginning of 2020** was the decoding of the three-dimensional structure of the main protease of the SARS-CoV2 virus, which was already achieved at BESSY II in February 2020. This protein is elementary in the life cycle of the coronavirus because it is involved in the reproduction of the viruses. Knowledge of its 3D structure helps in the search for suitable active substances that dock onto the protein and hinder its function. Because without information about the target protein, the search for an active agent is like looking for a needle in a haystack. Structure-based drug discovery" helps to identify the best candidates for active substances from the multitude of possible substances. > Read more here (news piece)
- **The BMBF is currently funding the two projects "CTS-COV-2" and "STOP CORONA"** at the two light sources PETRA III and BESSY II. In both projects, the main protease of the virus, which was decoded at BESSY II, was selected as the target for a drug.
  - In the STOP-CORONA project, which began as a collaboration between the Helmholtz-Zentrum Berlin (HZB), the University of Lübeck and the University of Würzburg, the aim is to use small organic substances, so-called fragments, to identify active surfaces of the main viral protease. For this fragment screening, the HZB has two libraries available F2X-Entry with 96 substances and F2X-Universal with 1103 substances.
    In a first step, crystals of the main protease were tested against the F2X-Entry library. From the binders obtained, a more strongly binding subsequent substance could be identified by optimisation. This substance is currently in binding studies and will be further optimised.
    These results provide important insights for drug discovery against SARS-CoV-2, as drugs are still urgently needed to get COVID19 under control. However, Corona research at synchrotrons is not limited to X-ray structure analysis.

RESEARCH

CORONAVIRUS

Crystal structure of SARS-CoV-2 main protease provides a basis for design of improved α-ketoamide inhibitors

Linlin Zhang[1,2], Daizong Lin[1,3], Xinyuanyuan Sun[1,2], Ute Curth[4], Christian Drosten[5], Lucie Sauerhering[6,7], Stephan Becker[6,7], Katharina Rox[8,9], Rolf Hilgenfeld[1,2]*

The coronavirus disease 2019 (COVID-19) pandemic caused by severe acute respiratory syndrome–coronavirus 2 (SARS-CoV-2) is a global health emergency. An attractive drug target among coronaviruses is the main protease (M^{pro}, also called $3CL^{pro}$) because of its essential role in processing the polyproteins that are translated from the viral RNA. We report the x-ray structures of the unliganded SARS-CoV-2 M^{pro} and its complex with an α-ketoamide inhibitor. This was derived from a previously designed inhibitor but with the P3-P2 amide bond incorporated into a pyridone ring to enhance the half-life of the compound in plasma. On the basis of the unliganded structure, we developed the lead compound into a potent inhibitor of the SARS-CoV-2 M^{pro}. The pharmacokinetic characterization of the optimized inhibitor reveals a pronounced lung tropism and suitability for administration by the inhalative route.

In December 2019, a new coronavirus caused an outbreak of pulmonary disease in the city of Wuhan, the capital of Hubei province in China, and has since spread globally (*1, 2*). The virus has been named severe acute respiratory syndrome–coronavirus 2 (SARS-CoV-2) (*3*) because the RNA genome is about 82% identical to that of the SARS coronavirus (SARS-CoV); both viruses belong to clade b of the genus *Betacoronavirus* (*1, 2*). The disease caused by SARS-CoV-2 is called coronavirus disease 2019 (COVID-19). Whereas at the beginning of the outbreak, cases were connected to the Huanan seafood and animal market in Wuhan, efficient human-to-human transmission led to exponential growth in the number of cases. On 11 March 2020, the World Health Organization (WHO) declared the outbreak a pandemic. As of 9 April, there were >1,500,000 cumulative cases globally, with a ~5.9% case fatality rate.

One of the best-characterized drug targets among coronaviruses is the main protease (M^{pro}, also called $3CL^{pro}$) (*4*). Along with the papain-like protease(s), this enzyme is essential for processing the polyproteins that are translated from the viral RNA (*5*). The M^{pro} operates at no fewer than 11 cleavage sites on the large polyprotein 1ab (replicase 1ab, ~790 kDa); the recognition sequence at most sites is Leu-Gln↓(Ser, Ala, Gly) (↓ marks the cleavage site). Inhibiting the activity of this enzyme would block viral replication. Because no human proteases with a similar cleavage specificity are known, such inhibitors are unlikely to be toxic.

Previously, we designed and synthesized peptidomimetic α-ketoamides as broad-spectrum inhibitors of the main proteases of betacoronaviruses and alphacoronaviruses as well as the 3C proteases of enteroviruses (*6*). The best of these compounds (**11r**; Fig. 1) showed an half-maximal effective concentration (EC_{50}) of 400 pM against Middle East respiratory syndrome–coronavirus (MERS-CoV) in Huh7 cells as well as low-μM EC_{50} values against SARS-CoV and a whole range of enteroviruses in various cell lines, although the antiviral activity seemed to depend to a great extent on the cell type used in the experiments (*6*). To improve the half-life of the compound in plasma, we modified **11r** by hiding the P3-P2 amide bond within a pyridone ring (Fig. 1, green ovals) in the expectation that this might prevent cellular proteases from accessing this bond and cleaving it. Further, to increase the solubility of the compound in plasma and to reduce its binding to plasma proteins, we replaced the hydrophobic cinnamoyl moiety by the somewhat less hydrophobic Boc group (Fig. 1, red ovals) to give **13a** (see scheme S1 for synthesis).

To examine whether the introduced pyridone ring is compatible with the three-dimensional structure of the target, we determined the crystal structure, at 1.75 Å resolution, of the M^{pro} of SARS-CoV-2 (Fig. 2). The three-dimensional structure is highly similar to that of the SARS-CoV M^{pro}, as expected from the 96% sequence identity (see fig. S8); the root mean square deviation between the two free-enzyme structures is 0.53 Å for all Cα positions [comparison between SARS-CoV-2 M^{pro} structure and SARS-CoV M^{pro}, PDB entry 2BX4 (*7*)]. The chymotrypsin-like and picornavirus 3C protease–like domains I and II (residues 10 to 99 and 100 to 182, respectively) are six-stranded antiparallel β barrels that harbor the substrate-binding site between them. Domain III (residues 198 to 303), a globular cluster of five helices, is involved in regulating the dimerization of the M^{pro}, mainly through a salt-bridge interaction between Glu^{290} of one protomer and Arg^{4} of the other (*8*). The tight dimer formed

[1]Institute of Biochemistry, Center for Structural and Cell Biology in Medicine, University of Lübeck, 23562 Lübeck, Germany. [2]German Center for Infection Research (DZIF), Hamburg-Lübeck-Borstel-Riems Site, University of Lübeck, 23562 Lübeck, Germany. [3]Changchun Discovery Sciences Ltd., 789 Shunda Road, Changchun, Jilin 130012, China. [4]Institute for Biophysical Chemistry, Hannover Medical School, 30625 Hannover, Germany. [5]Institute of Virology, Charité Universitätsmedizin Berlin, 10117 Berlin, Germany. [6]Institute of Virology, University of Marburg, 35043 Marburg, Germany. [7]German Center for Infection Research (DZIF), Marburg-Gießen-Langen Site, University of Marburg, 35043 Marburg, Germany. [8]Department of Chemical Biology, Helmholtz Center for Infection Research (HZI), 38124 Braunschweig, Germany. [9]German Center for Infection Research (DZIF), Hannover-Braunschweig Site, Helmholtz Center for Infection Research, 38124 Braunschweig, Germany.
*Corresponding author. Email: rolf.hilgenfeld@uni-luebeck.de

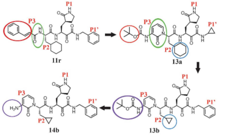

Fig. 1. Chemical structures of α-ketoamide inhibitors 11r, 13a, 13b, and 14b. Colored ovals and circles highlight the modifications from one development step to the next (see text).

Art and History

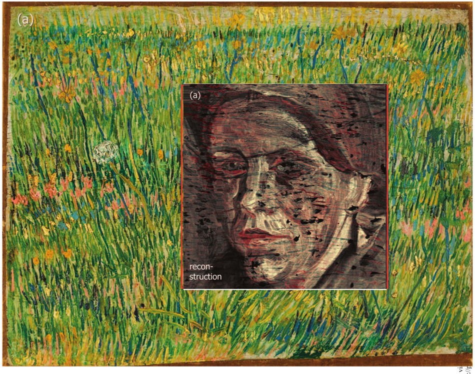

Anal. Chem. **2008,** *80,* 6436–6442

Visualization of a Lost Painting by Vincent van Gogh Using Synchrotron Radiation Based X-ray Fluorescence Elemental Mapping

Joris Dik,*,† Koen Janssens,‡ Geert Van Der Snickt,‡ Luuk van der Loeff,§ Karen Rickers,‖ and Marine Cotte ,⊗

Department of Materials Science, Delft University of Technology, Mekelweg 2, 2628CD Delft, The Netherlands, Centre for Micro- and Trace Analysis, Department of Chemistry, Universiteit Antwerpen, Universiteitsplein 1, 2610 Antwerp, Belgium, Kröller-Müller Museum, Houtkampweg 6, P.O. Box 1, 6730 AA Otterlo, The Netherlands, Deutsches Elektronen-Synchrotron (DESY), Notkestrasse 85, 22603 Hamburg, Germany, Centre of Research and Restoration of the French Museums, UMR-171-CNRS, Palais du Louvre, Porte des Lions, 14 quai François Mitterrand, 75001 Paris, France, and European Synchrotron Radiation Facility BP220, 38043 Grenoble Cedex, France

Vincent van Gogh (1853−1890), one of the founding fathers of modern painting, is best known for his vivid colors, his vibrant painting style, and his short but highly productive career. His productivity is even higher than generally realized, as many of his known paintings cover a previous composition. This is thought to be the case in one-third of his early period paintings. Van Gogh would often reuse the canvas of an abandoned painting and paint a new or modified composition on top. These hidden paintings offer a unique and intimate insight into the genesis of his works. Yet, current museum-based imaging tools are unable to properly visualize many of these hidden images. We present the first-time use of synchrotron radiation based X-ray fluorescence mapping, applied to visualize a woman's head hidden under the work *Patch of Grass* by Van Gogh. We recorded decimeter-scale, X-ray fluorescence intensity maps, reflecting the distribution of specific elements in the paint layers. In doing so we succeeded in visualizing the hidden face with unprecedented detail. In particular, the distribution of Hg and Sb in the red and light tones, respectively, enabled an approximate color reconstruction of the flesh tones. This reconstruction proved to be the missing link for the comparison of the hidden face with Van Gogh's known paintings. Our approach literally opens up new vistas in the nondestructive study of hidden paint layers, which applies to the oeuvre of Van Gogh in particular and to old master paintings in general.

Vincent van Gogh is generally recognized as one of the founding fathers of modern painting.[1] In recent decades his work has undergone extensive art historical and technical study. One striking feature that emerged is Van Gogh's frequent reuse of paintings in order to recycle the canvas.[2,3] The artist would simply paint a new composition on top of an existing work. This is usually attributed to the artist's lifelong economic hardship and the rapid, energetic evolution of his artistic ideas. Visualizing such hidden paintings is of interest to both specialists in the field of Van Gogh and the public alike. Covered paintings in general provide an insight into the making of artworks and the underlying conceptual changes. In the case of Van Gogh, they also present a touchstone for comparison with preparatory drawings and the abundant literary record. The extensive correspondence with his brother Theo van Gogh, an art dealer based in Paris, is full of remarks by Vincent on his work.

Nondestructive imaging of such hidden paint layers is usually realized by means of tube-based X-ray radiation transmission radiography (XRR). The absorption contrast in these images is mostly caused by the heavy metal components of pigments employed, such as lead in lead white or mercury in vermillion. Conventional XRR, however, has a number of important limitations. First of all, the observed X-ray absorbance is a summation of all element-specific absorbances. This implies that the contribution to the overall image contrast due to (low quantities of) weakly absorbing elements will frequently be obscured by heavier elements that are present in higher concentrations. Second, prior to the application of the paint layer, a canvas is usually primed with a homogeneous layer of lead white. This raises the overall background of the absorption image derived from the paint layers. Finally, the polychromatic character of an X-ray tube further reduces the contrast in radiographic images. As a result, conventional XRR imaging of paintings frequently provides only a fragmentary view of their substructure, which can severely hamper the readability of hidden compositions.[4]

* Corresponding author. Phone: +31-15-2789571. E-mail: j.dik@tudelft.nl.
† Delft University of Technology.
‡ Universiteit Antwerpen.
§ Kröller-Müller Museum.
‖ Deutsches Elektronen-Synchrotron (DESY).
Palais du Louvre.
⊗ European Synchrotron Radiation Facility.

(1) Hulsker, J. *The New Complete Van Gogh: Paintings, Drawings, Sketches*; John Benjamins: Philadelphia, PA, 1996.
(2) Van Heugten, S. *Van Gogh Museum J.* **1995**, 63–85.
(3) Hendriks, E. Van Gogh's Working Practice: A Technical Study. In *New Views on Van Gogh's Development in Antwerp en Paris: An Integrated Art Historical and Technical Study of His Paintings in the Van Gogh Museum*; Hendriks, E., Van Tilborgh, L., Eds.; University of Amsterdam: Amsterdam, The Netherlands, 2006; pp 231−245.
(4) Krug, K.; Dik, J.; Den Leeuw, M.; Whitson, A.; Tortora, J.; Coan, P.; Nemoz, C.; Bravin, A. *Appl. Phys. A: Mater. Sci. Process.* **2006**, *83*, 247–51.

10.1021/ac800965g CCC: $40.75 © 2008 American Chemical Society
Published on Web 07/29/2008

Accelerators for HEP

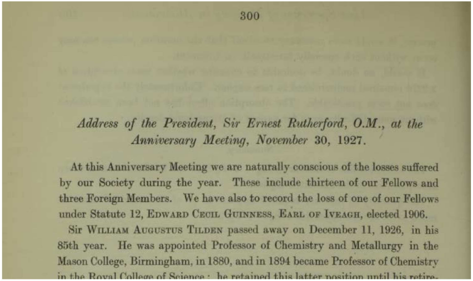

300

Address of the President, Sir Ernest Rutherford, O.M., at the Anniversary Meeting, November 30, 1927.

At this Anniversary Meeting we are naturally conscious of the losses suffered by our Society during the year. These include thirteen of our Fellows and three Foreign Members. We have also to record the loss of one of our Fellows under Statute 12, Edward Cecil Guinness, Earl of Iveagh, elected 1906.

Sir William Augustus Tilden passed away on December 11, 1926, in his 85th year. He was appointed Professor of Chemistry and Metallurgy in the Mason College, Birmingham, in 1880, and in 1894 became Professor of Chemistry in the Royal College of Science: he retained this latter position until his retire-

...

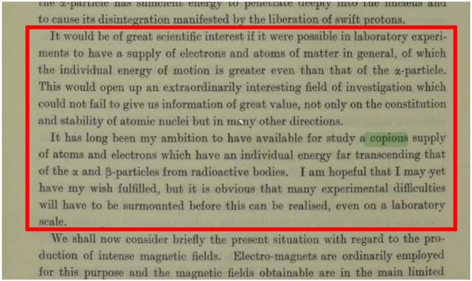

the α-particle has sufficient energy to penetrate deeply into the nucleus and to cause its disintegration manifested by the liberation of swift protons.

It would be of great scientific interest if it were possible in laboratory experiments to have a supply of electrons and atoms of matter in general, of which the individual energy of motion is greater even than that of the α-particle. This would open up an extraordinarily interesting field of investigation which could not fail to give us information of great value, not only on the constitution and stability of atomic nuclei but in many other directions.

It has long been my ambition to have available for study a copious supply of atoms and electrons which have an individual energy far transcending that of the α and β-particles from radioactive bodies. I am hopeful that I may yet have my wish fulfilled, but it is obvious that many experimental difficulties will have to be surmounted before this can be realised, even on a laboratory scale.

We shall now consider briefly the present situation with regard to the production of intense magnetic fields. Electro-magnets are ordinarily employed for this purpose and the magnetic fields obtainable are in the main limited

https://royalsocietypublishing.org/doi/pdf/10.1098/rspa.1928.0001

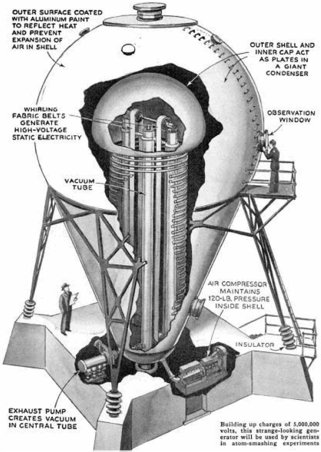

Westinghouse Atom Smasher, 5MeV
1937 – 1958, Pennsylvania, USA

For historical development of particle accelerators see, e.g.

P.J. Bryant, *A brief history and review of accelerators*, CERN Accelerator School: 5th General Accelerator Physics Course, Jyväskylä, Finland, Sep 1992 https://cds.cern.ch/record/261062/

Accelerators for HEP

⇨ Different types of collision

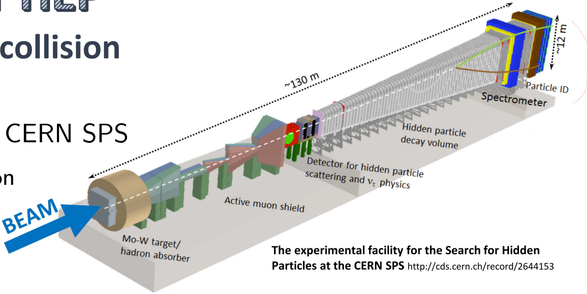

The experimental facility for the Search for Hidden Particles at the CERN SPS http://cds.cern.ch/record/2644153

Fixed target e.g. SHIP @ CERN SPS

- Simpler design/implementation → **cost!**
- Potential for very high intensity beams & large numbers of collissions

Collider e.g. LHC @ CERN

- More complex design + many extra challenges
- **LAB frame = CM frame** → maximum energy available for new particle creation

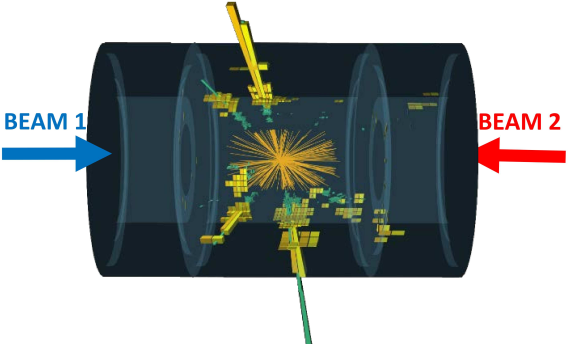

Accelerators for HEP ⇨ various accelerator geometry

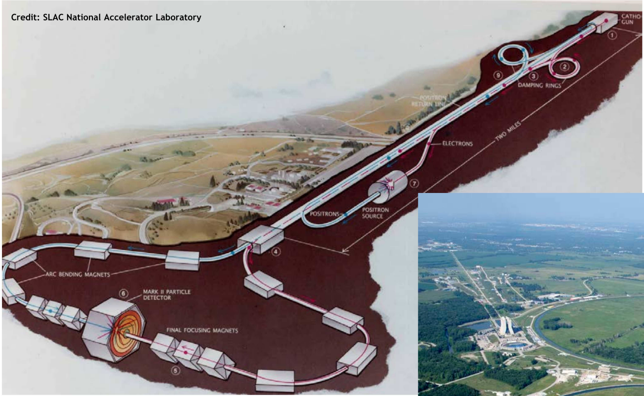

`Linear' collider
e.g. SLC

`Circular' collider
e.g. Tevatron

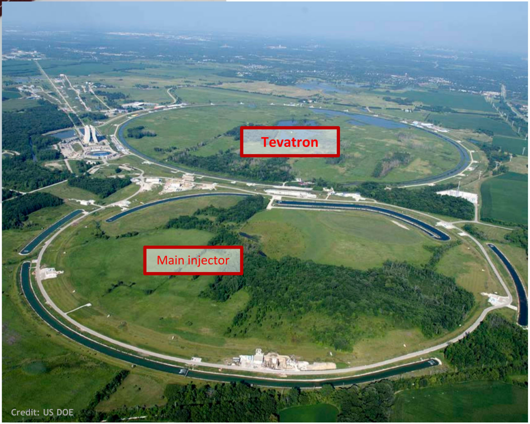

Accelerators for HEP ⇨ Different particle species

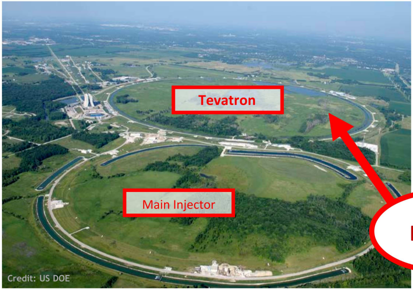

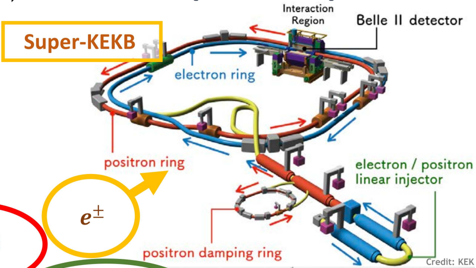

p or p̄

$e^{\pm}$

Lepton/Hadron

Heavy Ions

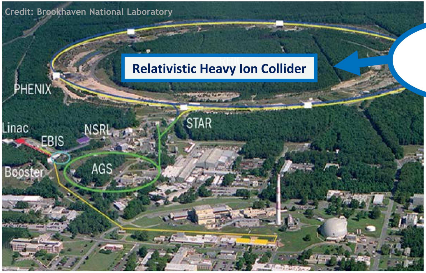

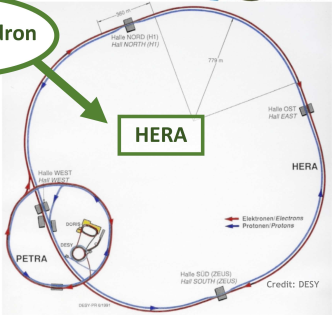

For overview of colliders see e.g. : V. Shiltsev and F. Zimmermann *`Modern and future colliders'* Rev. Mod. Phys. 93, 015006
https://journals.aps.org/rmp/abstract/10.1103/RevModPhys.93.015006

Accelerators for HEP ⇒ Large Hadron Collider (LHC) is the highest energy accelerator in operation today

27km superconducting synchrotron collider
(constructed in the former LEP tunnel)

Operated with various particle species:

- proton – proton
- Heavy ion (Pb^{82+} / Pb^{82+})
- Heavy ion (Xe^{54+} / Xe^{54+})
- Proton-lead (p / Pb^{82+})
- Partially stripped ions (Pb^{81+}) [non-colliding]
- *Possible future runs with oxygen & nitrogen*

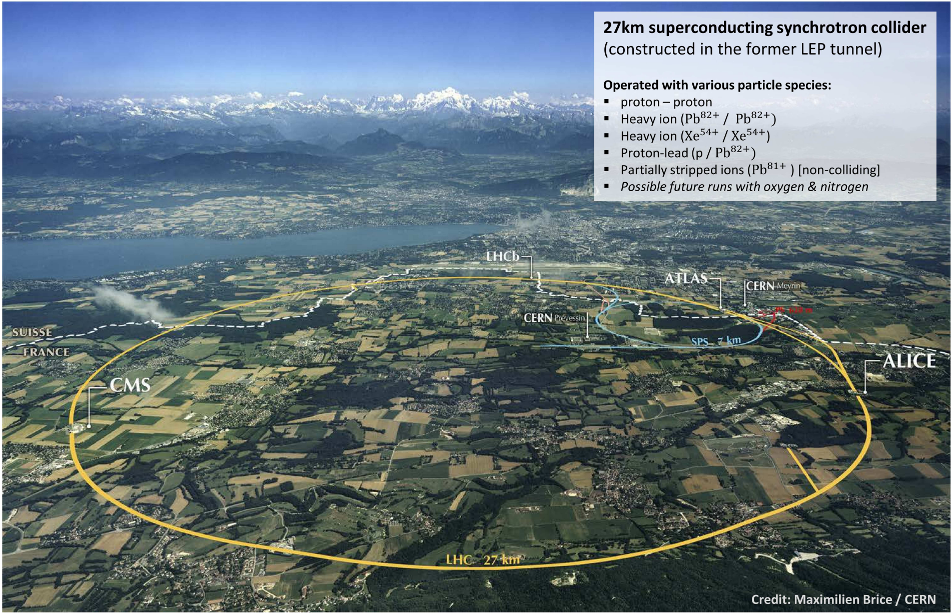

Credit: Maximilien Brice / CERN

The Large Hadron Collider (LHC)

- **2 counter-rotating beams in a twin-ring synchrotron**
- **8 straight insertion regions** (IRs) **& 8 bending Arcs** *'A12 → A81'*

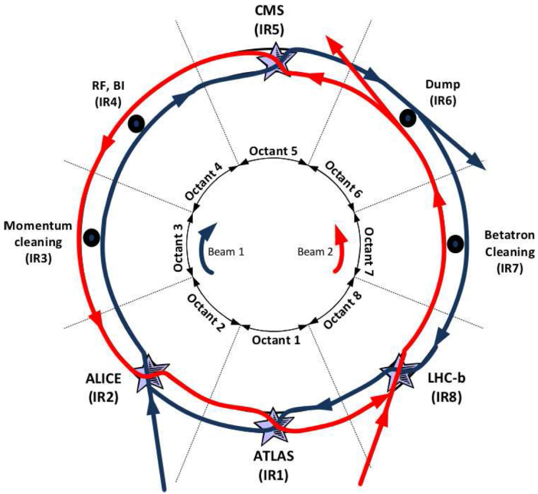

- **IR2:** LHC B1 injection + HEP (ALICE)
- **IR8:** LHC B2 injection + HEP (LHCb)

- **IR1:** HEP (ATLAS)
- **IR5:** HEP (CMS)

- **IR3:** COLLIMATION (momentum)
- **IR7:** COLLIMATION (transverse)

- **IR4:** Acceleration + instrumentation

- **IR6:** LHC B1+B2 BEAM DUMP

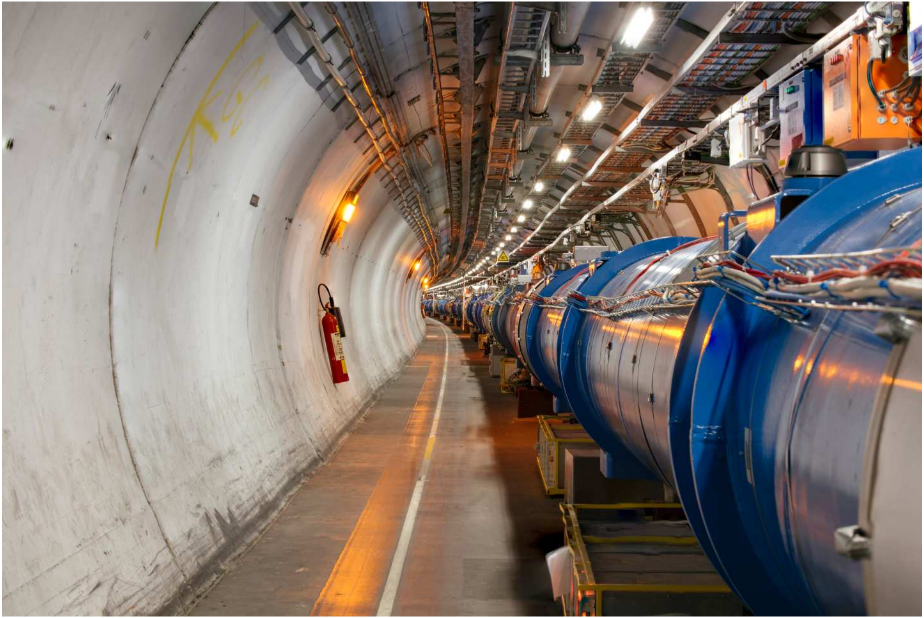

LHC arcs use ≈8T superconducting dual bore dipoles

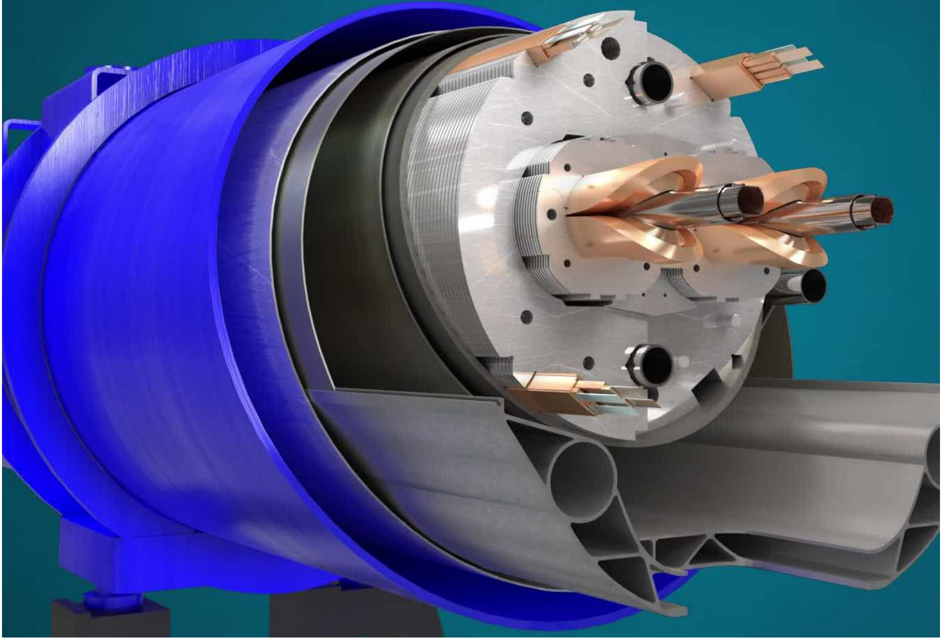

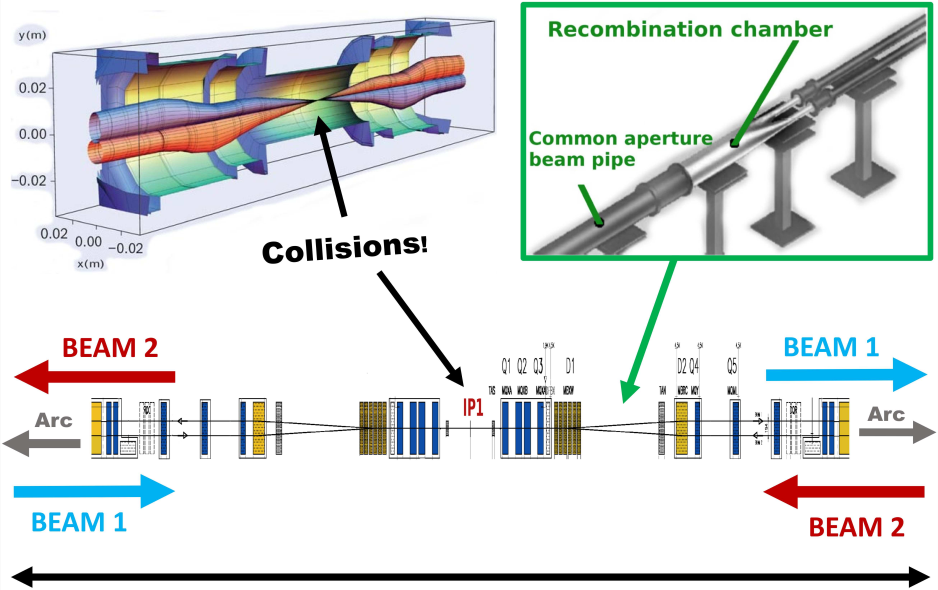

IR1 (ATLAS) from above

Accelerators for HEP

- **LHC has 2 injector chains**
- **Optimized to tackle different challenges at different energy scales & for protons-vs-heavy ions**

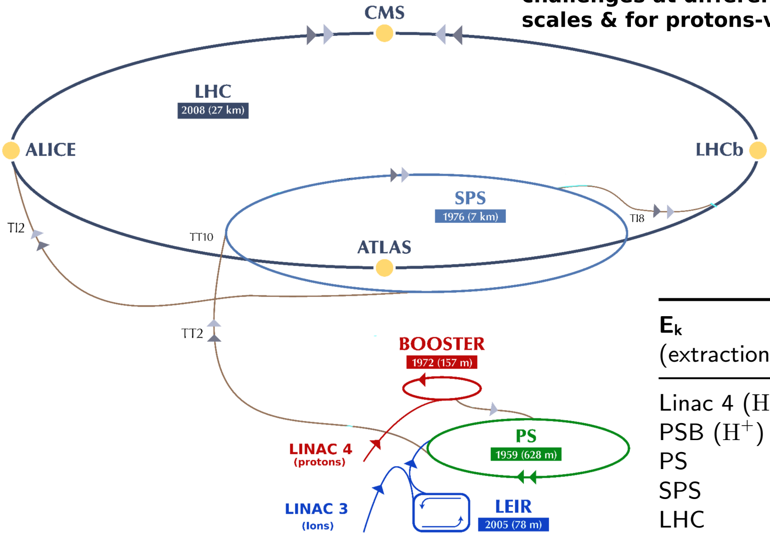

E_k (extraction)	post-LIU ($\geq$ 2020)
Linac 4 (H^-)	160 MeV
PSB (H^+)	2.0 GeV
PS	25 GeV
SPS	449 GeV
LHC	$\geq$ 6.8 TeV

The LHC cycle (2018)

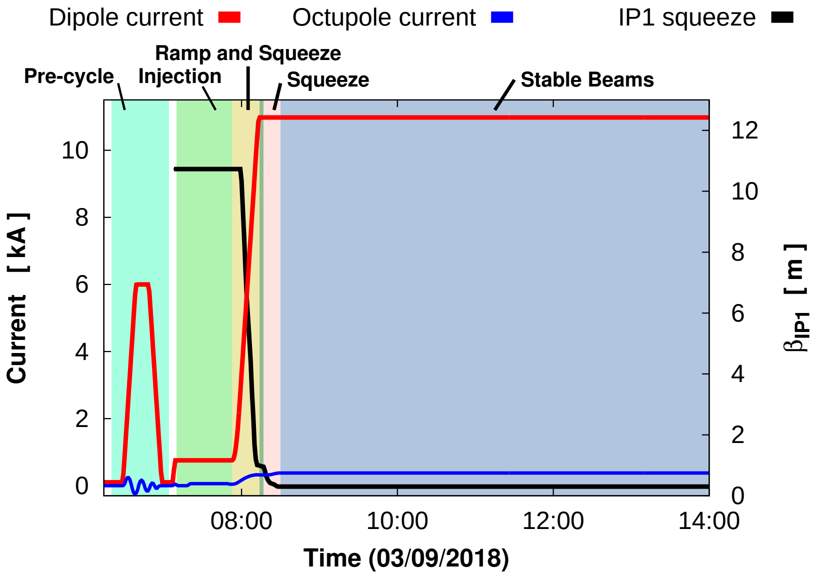

Key Points

- **Accelerators aren't just for HEP**
  - $\rightarrow$ *≈ 1/5 of Physics Nobel Prizes directly used an accelerator!*
  - $\rightarrow$ *Further 20 Nobel Prizes across Physics/Chemistry/Medicine have been awarded for research using X-rays!*
  - $\rightarrow$ https://www.epfl.ch/labs/lpap/wp-content/uploads/2018/10/AcceleratorsNobelPrizes.pdf
- **Accelerators for HEP come in a wide variety of flavours**
  - $\rightarrow$ specific design will depend on the HEP motivation
- **Current energy frontier machine is LHC**
- **LHC injector Chain, Layout and Cycle**

What do particle physicists care about??

Energy

Acceleration

$$\vec{F} = q(\vec{E} + \vec{v} \times \vec{B})$$

$$\Delta W = \int_{s_1}^{s_2} \boldsymbol{F}.\mathrm{d}\boldsymbol{s} = \int_{s_1}^{s_2} q\vec{E}.\mathrm{d}\vec{s}$$

- To accelerate charged particle do work via Lorentz force
- Magnetic field does no work $\vec{s}\,.\,(\frac{\mathrm{d}\vec{s}}{\mathrm{d}t} \times \vec{B}) = 0$

$$\vec{E} = -\nabla\phi - \frac{\partial \vec{A}}{\partial t}$$

Electrostatic accelerators

- **Acceleration via high DC voltage**

RF

- **Acceleration via time-varying fields**
- ***`radiofrequency technology'***

Electrostatic accelerators

e.g. Cockcroft-Walton (left), Van-de-Graff, …

- **Limited by DC-breakdown voltage**
- **Can't be used for repeated acceleration around a closed loop** (e.g. in a synchrotron)

$$\oint \nabla\phi . \mathrm{d}\vec{s} = 0$$

- **Critical element in the design of particle sources**

RF Cavities

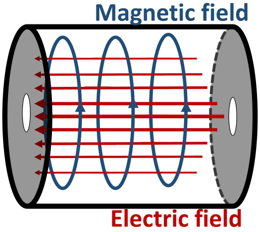

- Basis of all modern high-energy accelerators
- Conducting cavity or waveguide enforces boundary conditions which have solution with an accelerating mode

There are many varieties of RF-cavity:

e.g. travelling wave structures

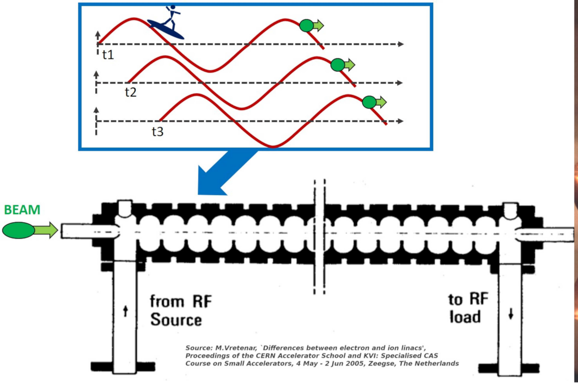

Source: M.Vretenar, `Differences between electron and ion linacs', Proceedings of the CERN Accelerator School and KVI: Specialised CAS Course on Small Accelerators, 4 May - 2 Jun 2005, Zeegse, The Netherlands

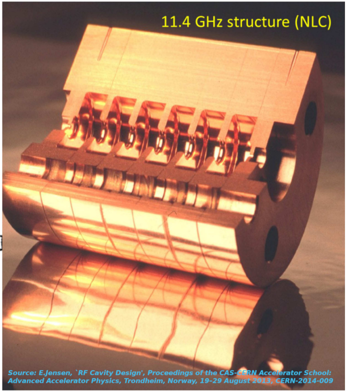

Source: E.Jensen, `RF Cavity Design', Proceedings of the CAS-CERN Accelerator School: Advanced Accelerator Physics, Trondheim, Norway, 19-29 August 2013, CERN-2014-009

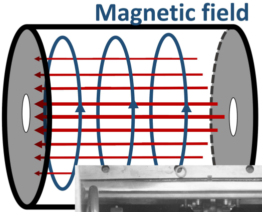

RF Cavities

There are many varieties of RF-cavity:

e.g. standing wave drift tube Alvarez structure

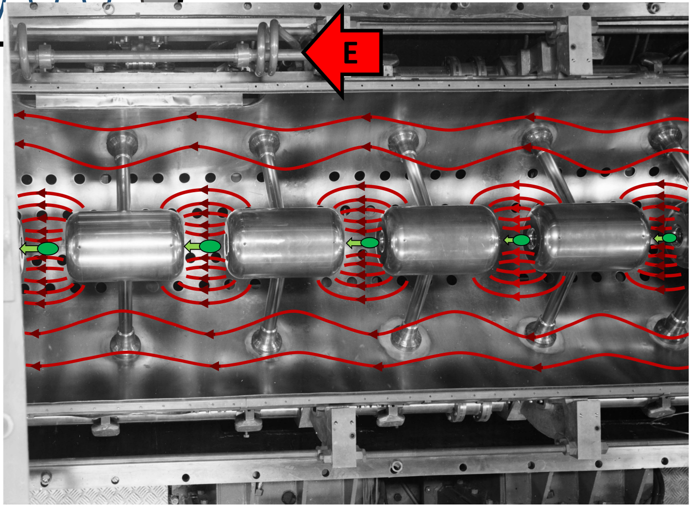

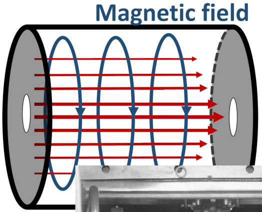

RF Cavities

There are many varieties of RF-cavity:

e.g. standing wave drift tube Alvarez structure

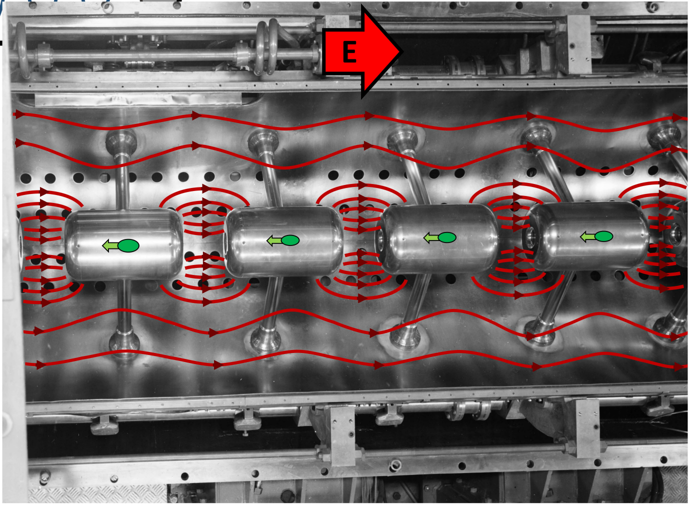

RF Cavities

There are many varieties of RF-cavity:

e.g. superconducting elliptical cavity (LHC)

- RF frequency is harmonic of revolution frequency

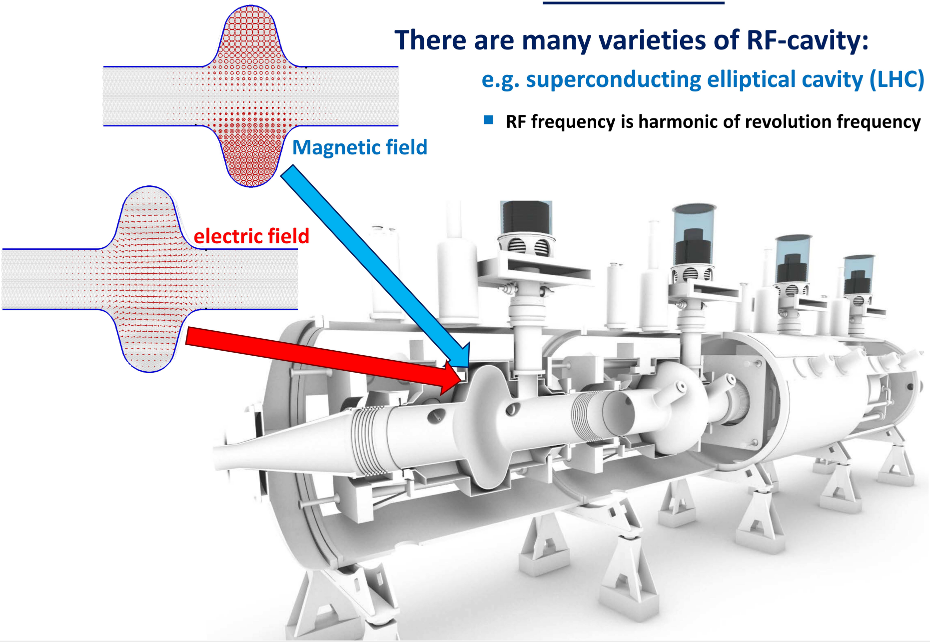

All RF cavities in the LHC are located at IR4

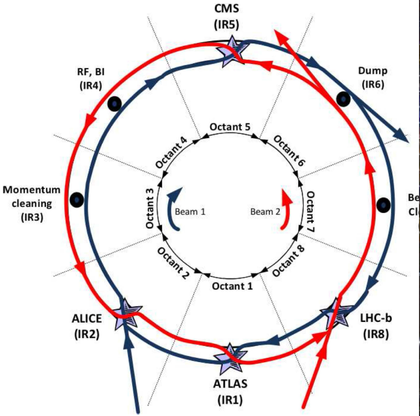

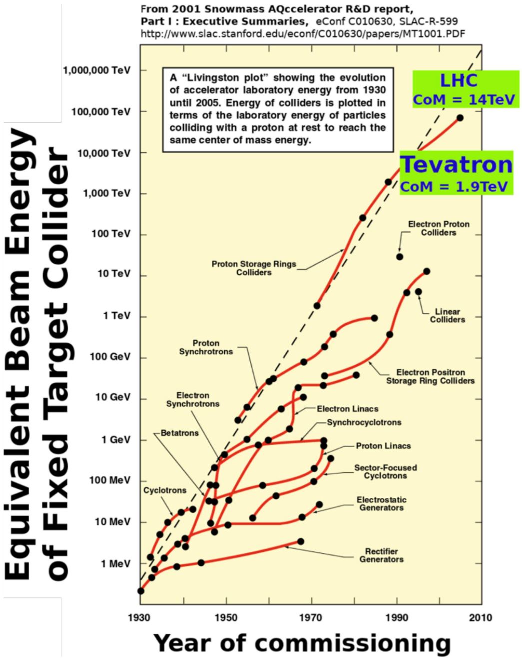

Beam-beam collider is essential for operation at energy frontier

Fixed target CoM energy:

$$E_{CM} \approx \sqrt{2 m_t E_b}$$

Collider CoM energy:

(head-on, equal mass)

$$E_{CM} = 2E_b$$

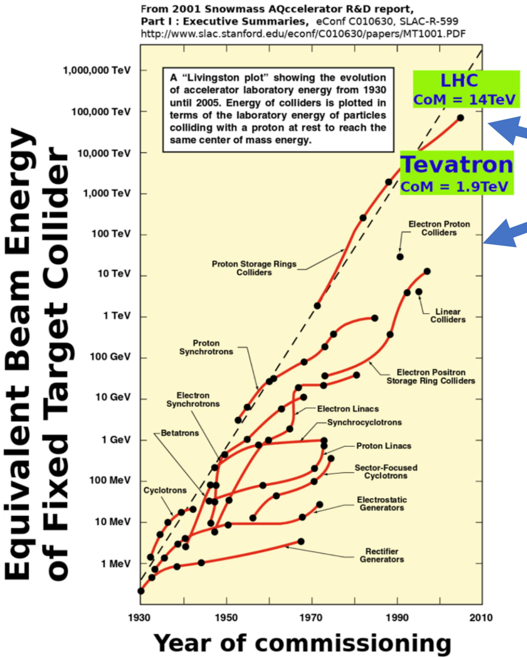

Clear distinction between energies achieved with $e^{\pm}$ vs hadron colliders

Limiting factor for circular e^+ / e^- accelerators:

→ particles emit **synchrotron radiation** as they are bent around ring

$$\Delta E/\mathrm{turn} \propto \frac{(\beta_{rel}\gamma_{rel})^4}{\rho}$$

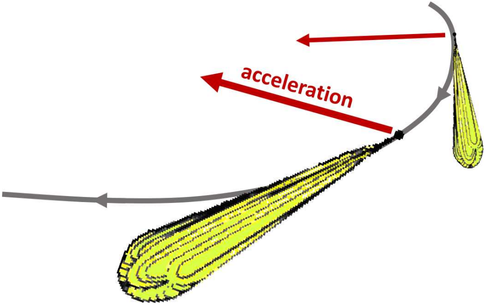

- **LEP** (e) **energy loss:** $\sim 3\,\mathrm{GeV/turn}$ (@ $101\,\mathrm{GeV}$)
- **LHC** (p) **energy loss:** $\sim 5\,\mathrm{keV/turn}$ (@ $6.5\,\mathrm{TeV}$)

To achieve higher energy-scales with $e^{\pm}$ need to significantly increase the bending radius and circumference!

- **FCC-ee:** 100km, $88 - 365 GeV$ e^+/e^- collider)
- similar CEPC project in proposed in China

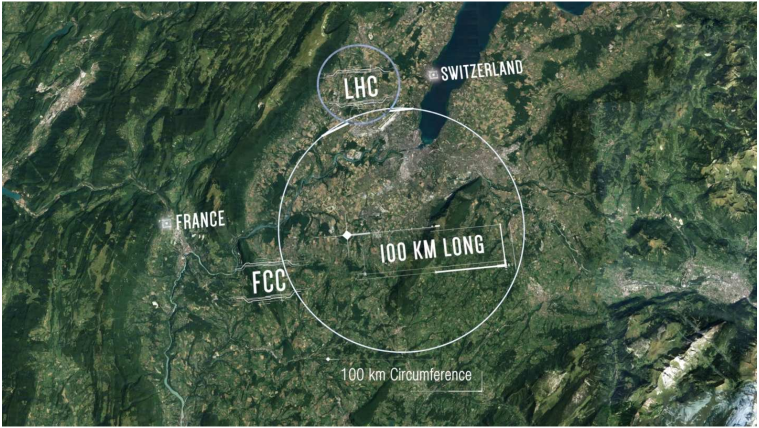

Even at 100km energy-loss/turn 3-4× more than LEP!
→ design challenging as beam-energy changes around the ring!

Several proposals for next-generation linear colliders!

- **Not limited by synchrotron radiation**
- **Energy limited by collider length and accelerating gradient!**
- **Lots of research into high-gradient RF cavities to produce high-quality electron beams!**

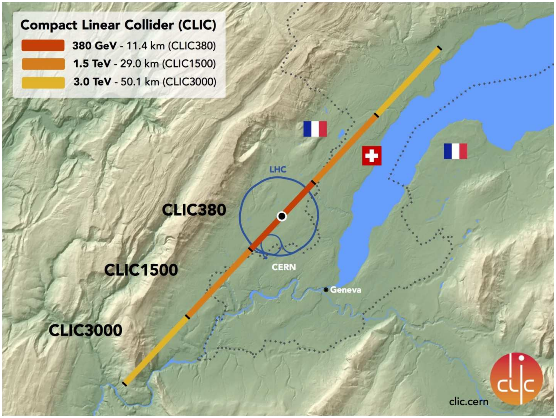

- **CLIC:** 11km/380GeV
- **CLIC:** up to 50km/3TeV)
- **similar ILC project proposed in Japan**

- **Would take lots of power to drive RF cavities for CLIC: conventional supplies can't cope!**
- **CLIC: a particle accelerator powering a particle accelerator!**

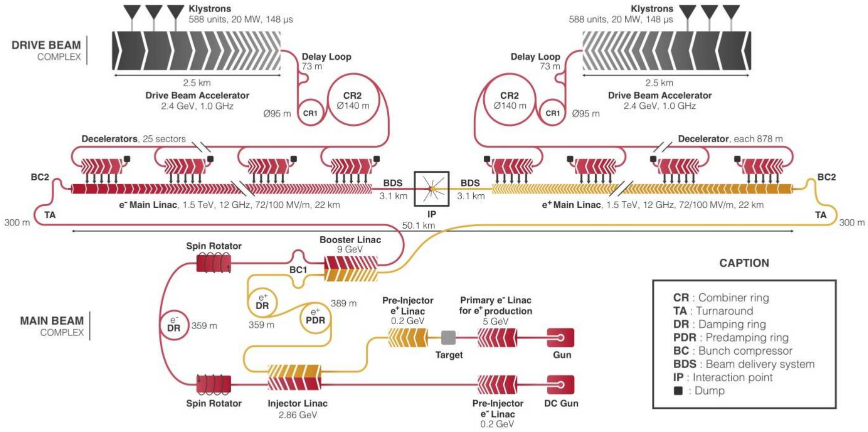

Limiting factor for circular hadron collider:

$$\vec{\mathbf{F}} = q(\vec{\mathbf{E}} + \vec{\mathbf{v}} \times \vec{\mathbf{B}})$$

- **Use Lorentz force to deflect beams around the synchrotron ring**

Must create strong enough magnetic field to bend beams around whatever radius is defined by the tunnel geometry

$$\mathbf{F}_{Lorentz} = \mathbf{F}_{centrip}$$

$$qvB = \frac{\gamma m_{rest} v^2}{\rho} = \frac{pv}{\rho}$$

$$B\rho = \frac{p}{q}$$

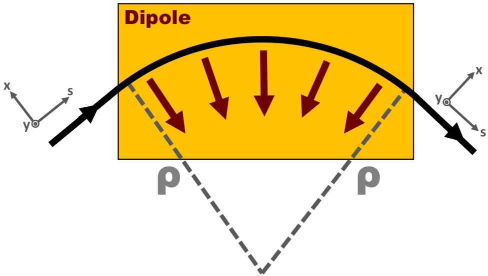

Limiting factor for circular hadron collider:

→ **need sufficient magnet strength to bend beams around the ring**

$$B\rho \ \ [\mathrm{Tm}] = \frac{p \ \ [\mathrm{kgms}^{-1}]}{q \ \ [\mathrm{C}]}$$

$$B\rho \ \ [\mathrm{Tm}] = \frac{10}{2.998} p \ [GeV/c]$$

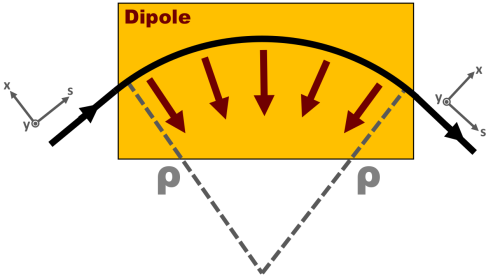

Bρ is 'magnetic rigidity': defines the maximum energy you can reach for a given dipole field in a given tunnel geometry

To go to higher-energy scales with $p^{\pm}$:

- significant increase to circumference
- significant increases to magnetic field

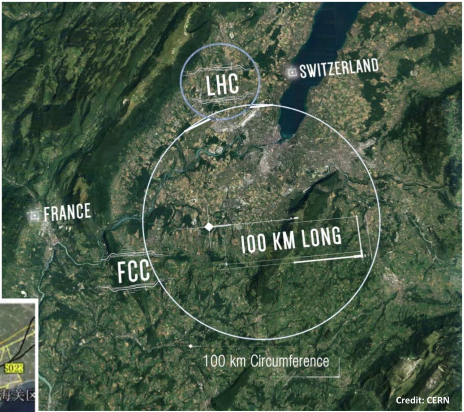

For more details:
Future Circular Collider Conceptual Design Report Volume 3
https://link.springer.com/article/10.1140/epjst/e2019-900087-0

Figure 3.3: Illustration of the CEPC-SPPC ring sited in Qinghuangdao. The small circle is 50 km, and the big one 100 km. Which one will be chosen depends on the funding scenario.

For more details:
CEPC-SPPC Preliminary Conceptual Design Report. 2. Accelerator
https://inspirehep.net/literature/1395736

CEPC Conceptual Design Report: Volume 1 – Accelerator
https://arxiv.org/abs/1809.00285

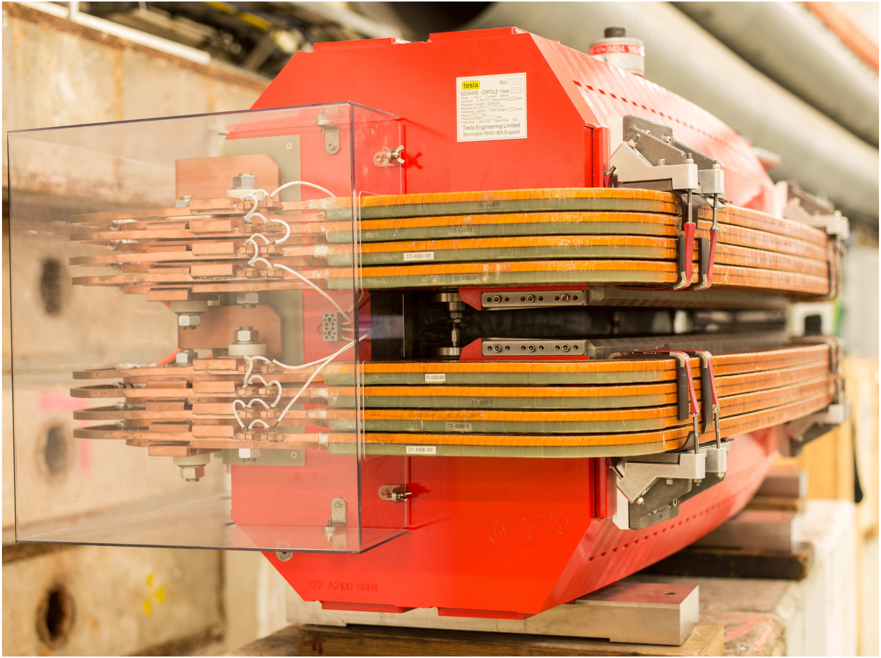
tesla
No:
SESAME - DIPOLE Year:
Field: 1.455 T Current: 494 A
Gradient: -2.79 T/m Inductance: mH
Magnetic Length: 2250 mm
Resistance @ 20°C: mΩ
Aperture: 40mm Yoke Length: mm
Mass: kg
Pressure Drop: bar
Flow Rate: 29L/min Temp Rise: 10°C
Tesla Engineering Limited
Storrington RH20 3EA England

- **Conventional dipole field defined by core**
- **Conventional dipoles limited to $\sim 2\,\mathrm{T}$ by saturation of core**

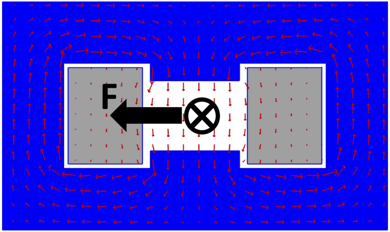

- $> 2\,\mathrm{T}$ **need very large current** $\rightarrow$ **superconductors!!!!**
- **Field defined by coil geometry** $\rightarrow$ **I $\propto$ cos Θ**

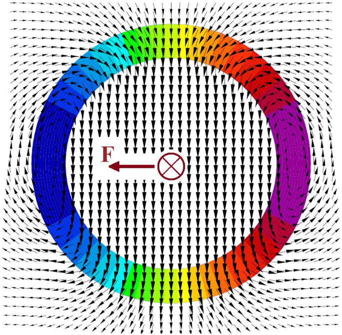

For discussion of magnet design: **S.Russenschuck**, **Design of accelerator magnets**, CERN accelerator school, Loutraki, Greece, Oct' 2000 https://cds.cern.ch/record/865932

- **Conventional dipole field defined by core**
- **Conventional dipoles limited to $\sim 2\,\mathrm{T}$ by saturation of core**

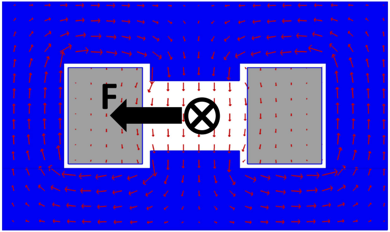

- $> 2\,\mathrm{T}$ **need very large current** $\rightarrow$ **superconductors!!!!**
- **Field defined by coil geometry** $\rightarrow$ **I** $\propto$ **cos** Θ

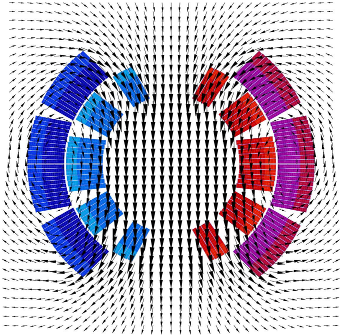

For discussion of magnet design: **S.Russenschuck**, **Design of accelerator magnets**, CERN accelerator school, Loutraki, Greece, Oct' 2000 https://cds.cern.ch/record/865932

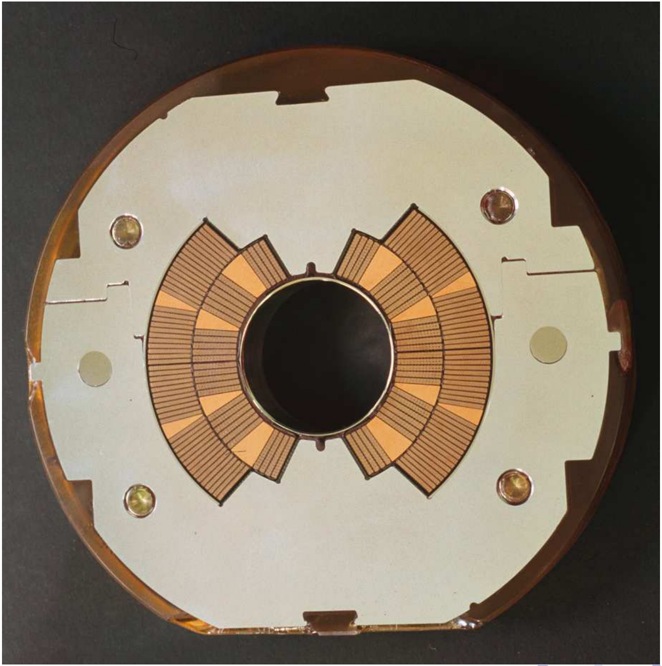

LHC arcs use ≈8T superconducting dual bore dipoles

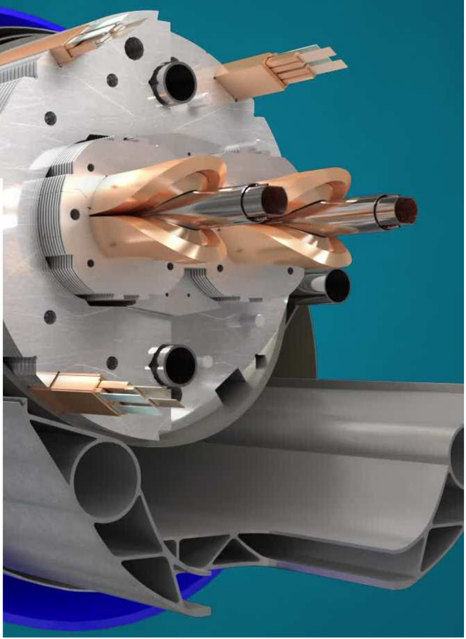

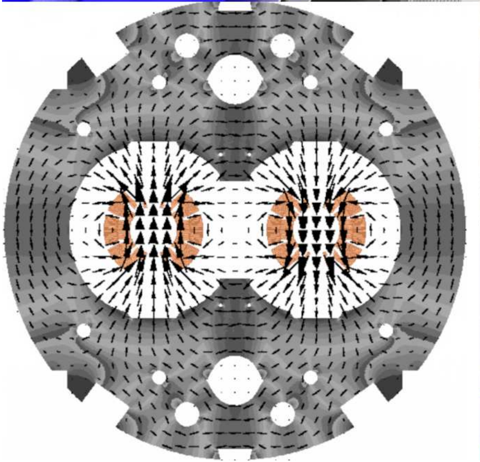

But what about the moon?

Credit: NASA/Goddard Space Flight Center/Arizona State University

Tidal deformation of earths crust changes the LHC circumference

→ **If uncorrected this causes a drift in the beam energy**

Effect of terrestrial tides on the LEP beam energy
L. Arnaudon et al. CERN SL/94-07 http://cds.cern.ch/record/260368

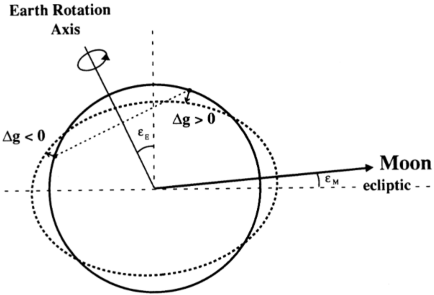

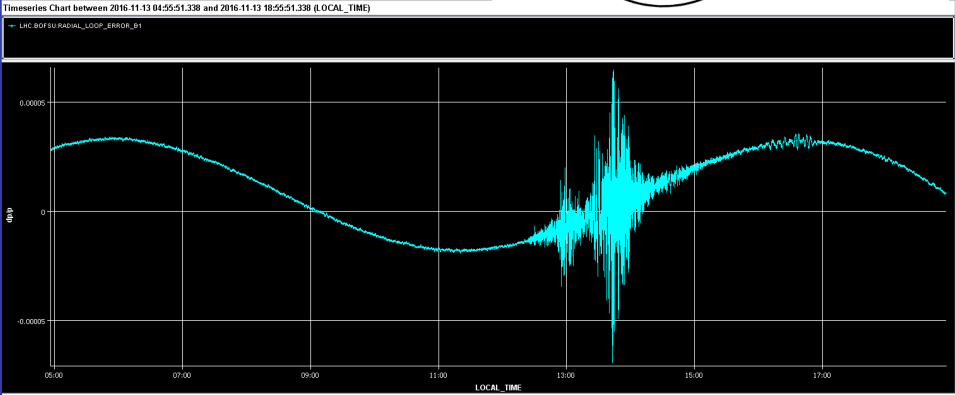

SC-magnets must be trained to reach higher fields/currents

- **Time needed for training was a key factor in the choice of LHC energy in Run2 and Run3**

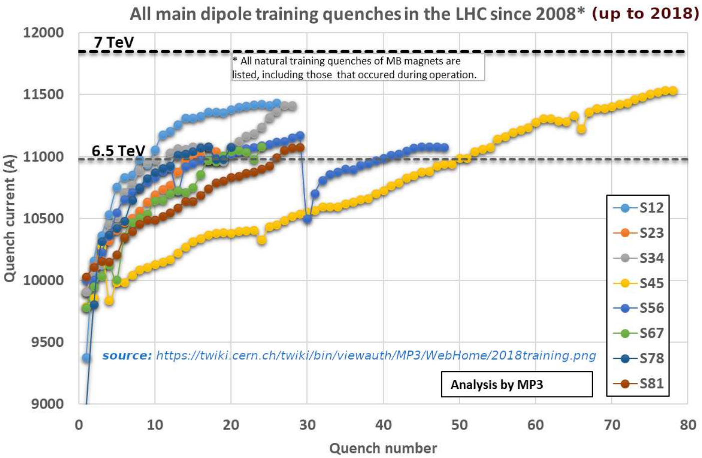

High-energy beams plus extremely high stored energy in magnets poses serious challenges for machine protection

Report of the Task Force on the Incident of 19th September 2008 at the LHC", CERN-LHC-PROJECT-Report-1168:

"The dipole bus bar at the location of the arc was vaporized, as well as the M3 line bellows around it, thus breaking open the helium enclosure..."

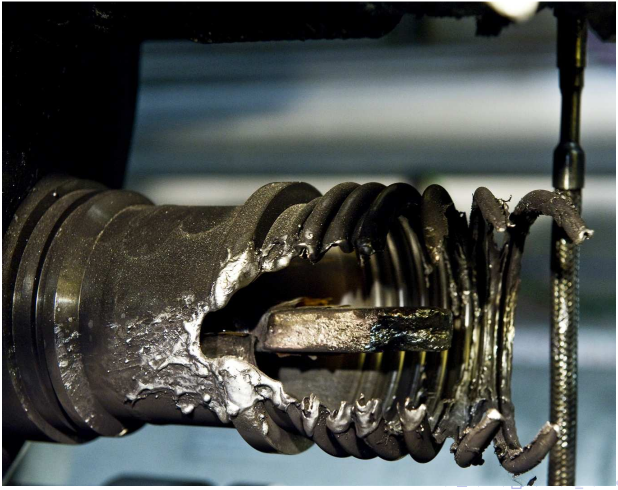

High-energy beams plus extremely high stored energy in magnets poses serious challenges for machine protection

Report of the Task Force on the Incident of 19th September 2008 at the LHC", CERN-LHC-PROJECT-Report-1168:

"The force was applied to the external support jacks, displacing the cryomagnets from them and in some cases, rupturing their ground anchors or the concrete in the tunnel floor."

Key Points

- **Use RF cavities to accelerate the beams**
- **Use dipole magnets to bend beam around the ring**
- **Different limitations on beam-energy for $e^{\pm}$ and hadron accelerators**
- **Various options being explored for next energy frontier accelerator**
- **Real world effects pose various challenges w.r.t. beam energy!**

What do particle physicists care about???

→ How much data (how many collisions) are generated?

Luminosity

Event rate for a HEP interaction:

$$\mathbf{R} = \mathbf{L} \times \boldsymbol{\sigma}$$

- **R:** *Event Rate* $[\mathbf{s}^{-1}]$
- $\boldsymbol{\sigma}$**:** *Cross Section* $[\mathbf{barn} = \mathbf{10^{-24} cm^2}]$
  property of the HEP interaction
- **L:** *Luminosity* **[inverse barn / s]**
  property of the collider

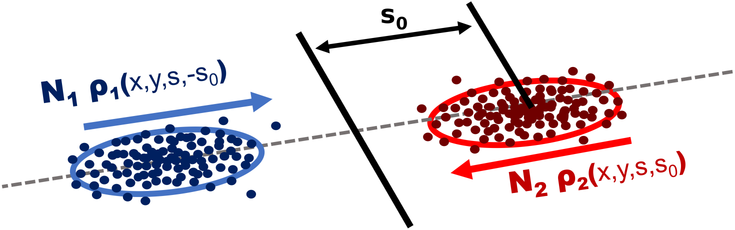

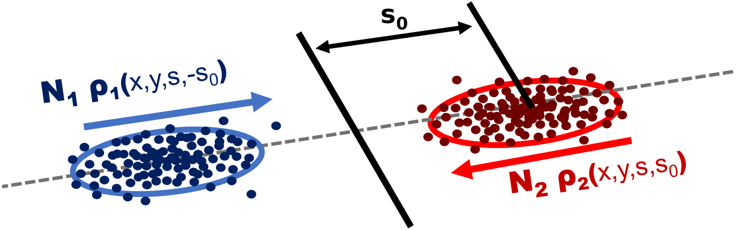

$$\mathbf{L} = f\sqrt{(\bar{v}_1-\bar{v}_2)^2-(\bar{v}_1\times\bar{v}_2)^2\ /\ c^2}\ N_1 N_2 \iiiint_{-\infty}^{+\infty} \rho_1(x,y,s,-s_0)\rho_2(x,y,s,s_0)\,\mathrm{d}x\,\mathrm{d}y\,\mathrm{d}s\,\mathrm{d}s_0$$

For detailed discussion of Luminosity relations:

W.Herr & B.Muratori, *Concept of Luminosity*, CERN Accelerator School, Zeuthen, Germany, 15 - 26 Sep 2003

Toshio Suzuki, *General Formulas of Luminosity for Various Types of Colliding Beam Machines*, KEK-76-3, (1976)

M.A. Furman, *The Møller Luminosity Factor*, LBNL-53553,CBP Note-543, September 24, 2003

C.Møller, *General properties of the characteristic matrix in the theory of elementary particles I*,
K. Danske Vidensk. Selsk. Mat.-Fys. Medd. 23, 1 (1945) http://gymarkiv.sdu.dk/MFM/kdvs/mfm 2020-29/mfm-23-1.pdf

with some approximation:

$$\mathbf{L} = \frac{\left(f_{rev} n_{coll}\right) \; N_1 N_2}{2\pi \sqrt{\left(\sigma_{x,1}^2 + \sigma_{x,2}^2\right)} \sqrt{\left(\sigma_{y,1}^2 + \sigma_{y,2}^2\right)}}$$

Assume:

- **uncorrellated gaussian bunch profiles in x,y,s**
- **head-on colinear collission of equal/opposite velocity beams**
- **equal bunch lengths** $\sigma_{s,1} \approx \sigma_{s,2}$
- **revolution frequency of 2 beams are in sync**
- n_{coll} **colliding bunches are all described by similar** $N_{1,2}, \sigma$

$$\mathbf{L} = \frac{(f_{rev} n_{coll})\ N_1 N_2}{2\pi\sqrt{(\sigma^2_{x,1} + \sigma^2_{x,2})}\sqrt{(\sigma^2_{y,1} + \sigma^2_{y,2})}}$$

Beamsize:

$$\boldsymbol{\sigma}_{\mathbf{x,y}} = \sqrt{\boldsymbol{\beta}_{\mathbf{x,y}}\mathbf{(s)}\ \boldsymbol{\epsilon}_{\mathbf{x,y}}}$$

- β**(s):** *'beta-function'* [**m**]
  $\rightarrow$ **Property of the magnetic lattice**
  $\rightarrow$ **varies around the ring**
- ϵ**:** *'emittance'* [μ**m**]
  $\rightarrow$ **Property of the particle bunch**
  $\rightarrow$ **Invariant around the ring**

- **Use quadrupole fields to focus particle beams and control the beam-size**

  $\rightarrow$ **F** $\propto$ displacement from center

  $\rightarrow$ **I** $\underset{\sim}{\propto}$ **cos** 2Θ

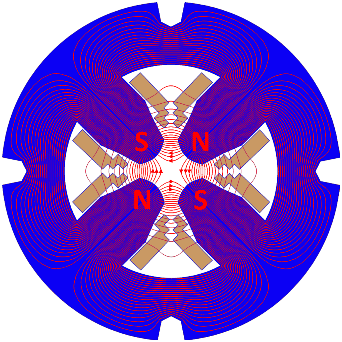

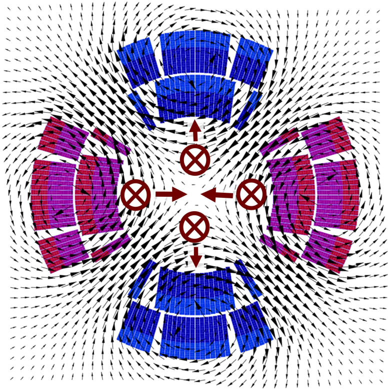

For discussion of magnet design: **S.Russenschuck**, **Design of accelerator magnets**, CERN accelerator school, Loutraki, Greece, Oct' 2000 https://cds.cern.ch/record/865932

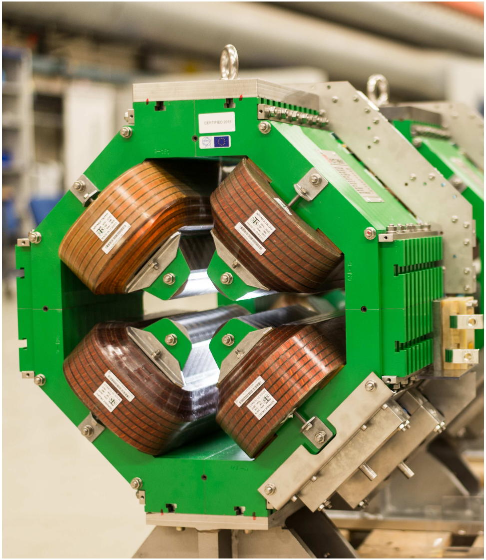

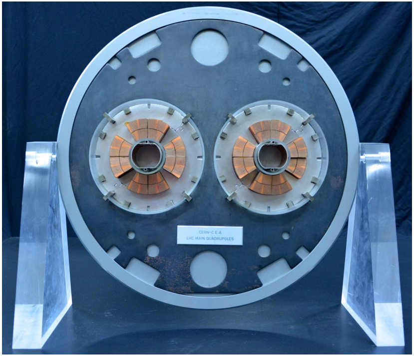
CERN-C.E.A
LHC MAIN QUADRUPOLES

- **Single quadrupole can focus in either H or V. Not both.**
- **Use alternating lattice of focusing/defocusing quads**

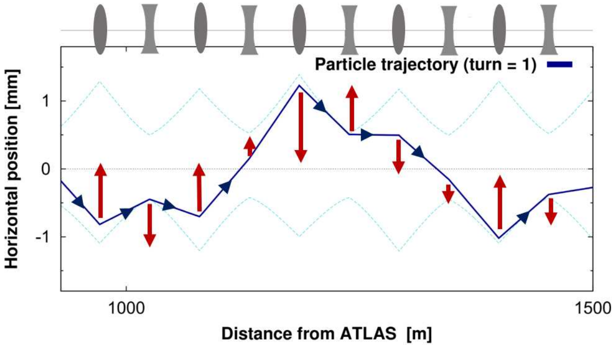

- **Particle will oscillate around central orbit, within an envelope defined by the β function**

$$x = \sqrt{2J_x\beta_x(s)}\cos\left(\phi_x(s) + \phi_0\right) \quad (1)$$

β-function describes envelope of particle oscillations

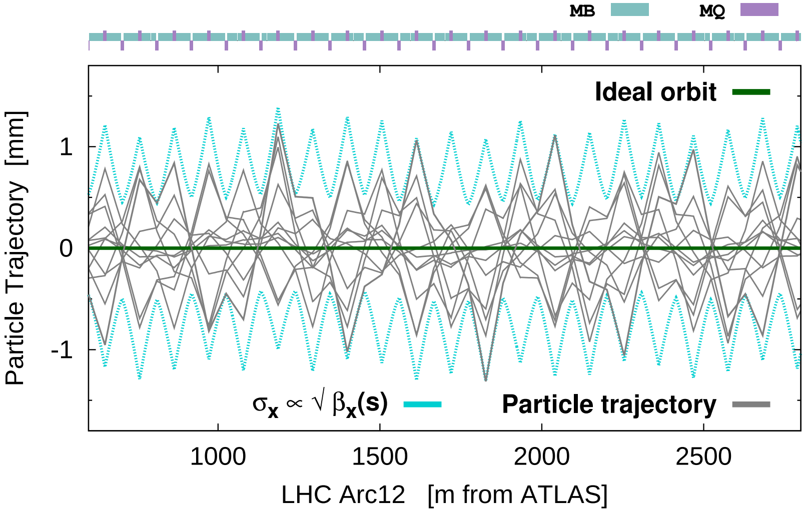

β-function describes envelope of particle oscillations

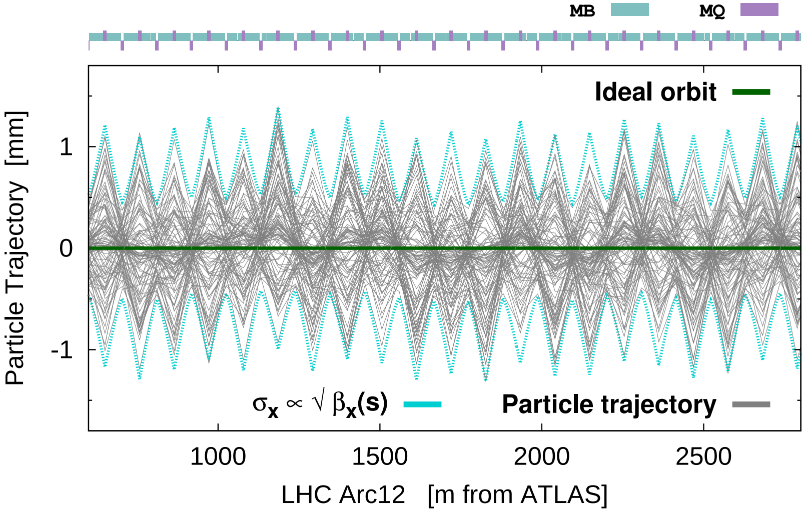

β-function describes envelope of particle oscillations

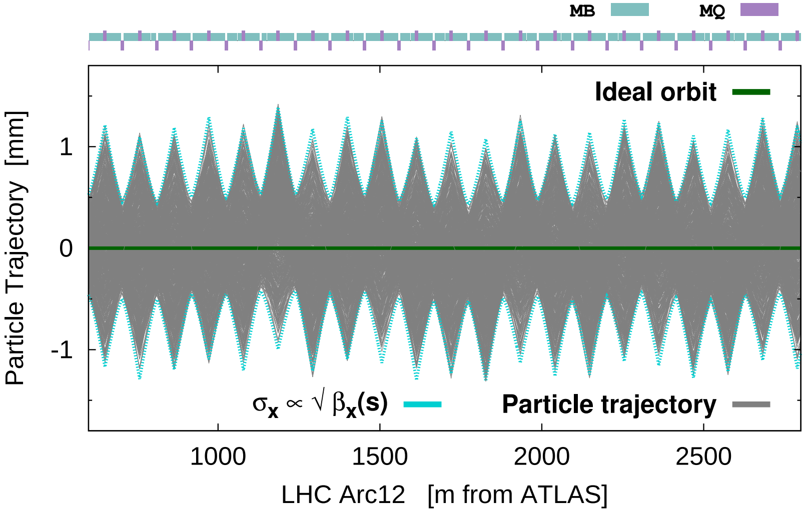

Triplet quadrupoles in experimental IRs squeeze $\beta_{x,y}$

$\rightarrow$ $\boldsymbol{\beta^*}$ $=$ minimum β in the IR $\approx 25\,\mathrm{cm}$

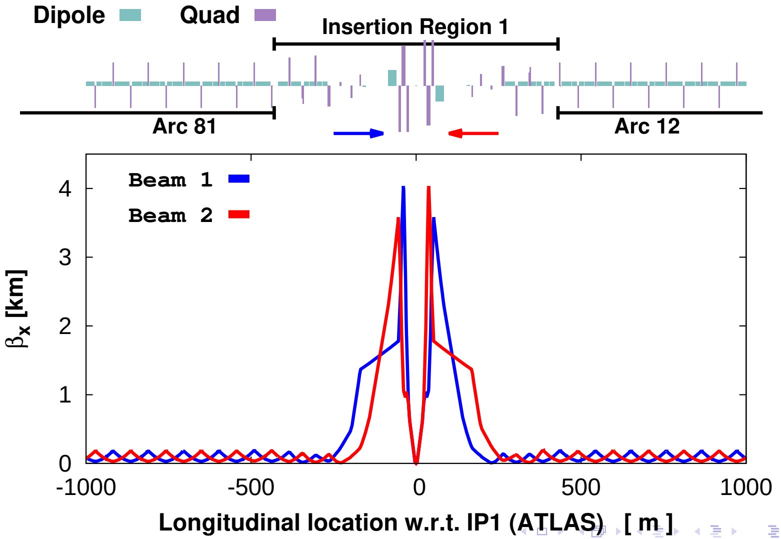

Around 2026-27 LHC will shut down for major upgrades into the High-Luminosity-LHC

- **Installation of new triplet magnets (Nb_3Sn) allowing further reduction of β**
- **Testing and construction ongoing!**

Characterise particle trajectory by position (x) and angle ($x' = \frac{\mathrm{d}x}{\mathrm{d}s}$)

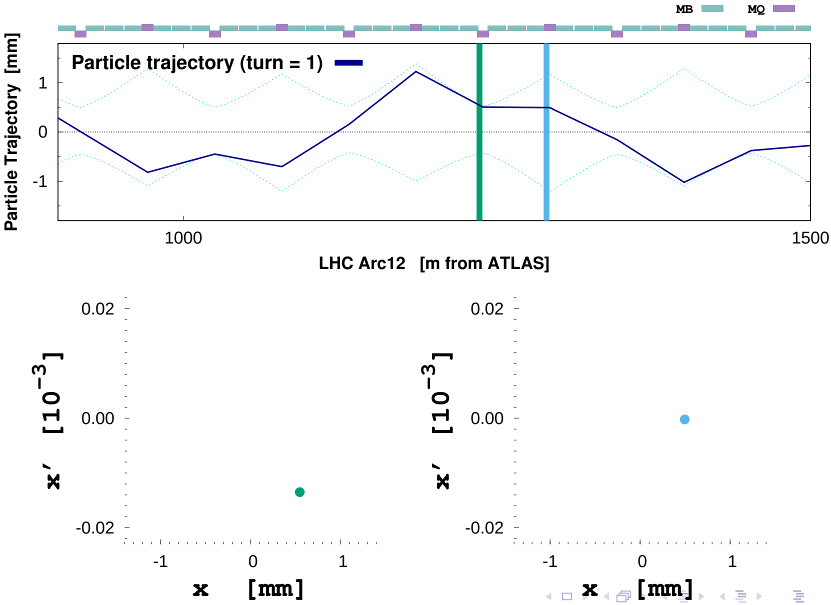

Characterise particle trajectory by position (x) and angle ($x' = \frac{dx}{ds}$)

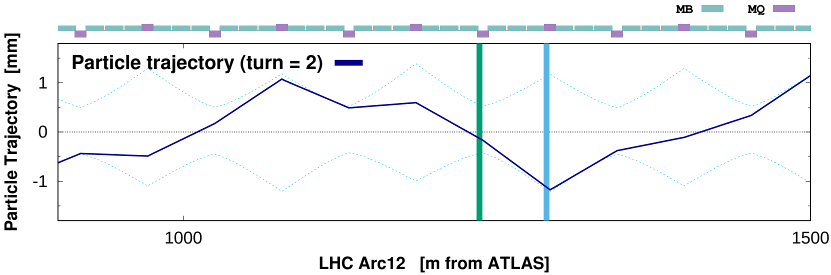

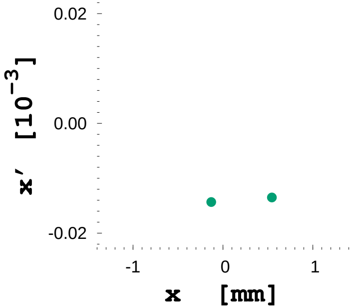

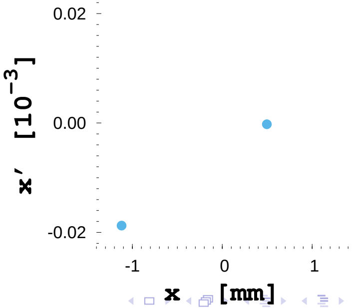

Characterise particle trajectory by position (x) and angle ($x' = \frac{dx}{ds}$)

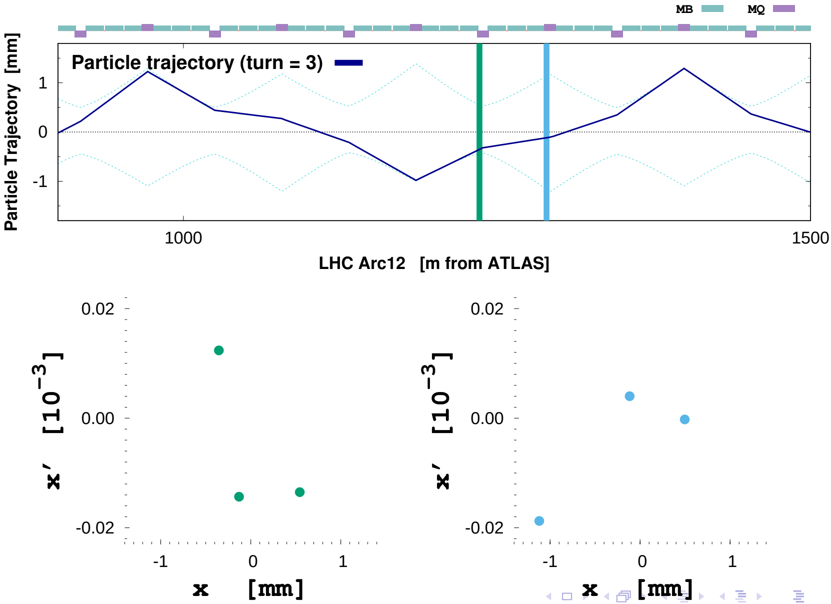

Characterise particle trajectory by position (x) and angle ($x' = \frac{dx}{ds}$)

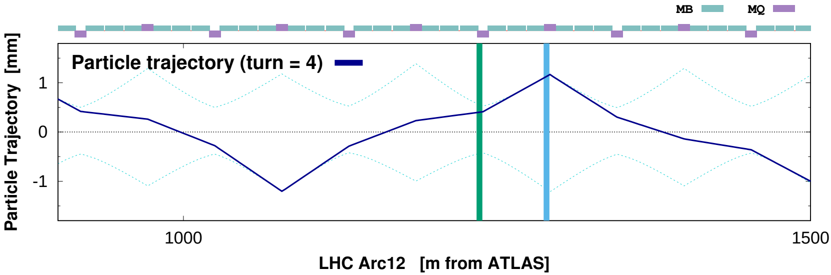

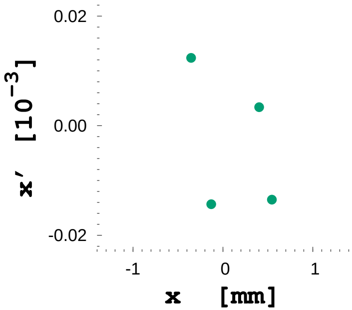

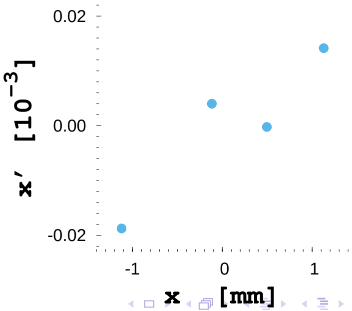

Characterise particle trajectory by position (x) and angle ($x' = \frac{dx}{ds}$)

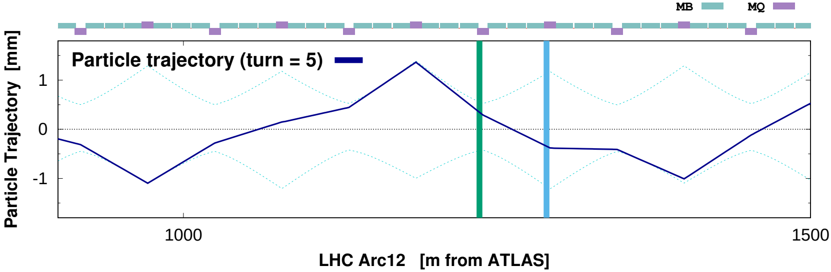

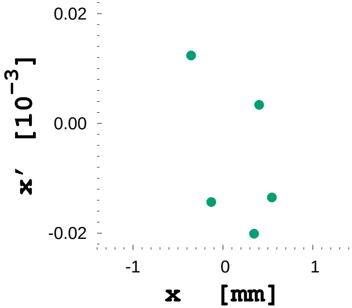

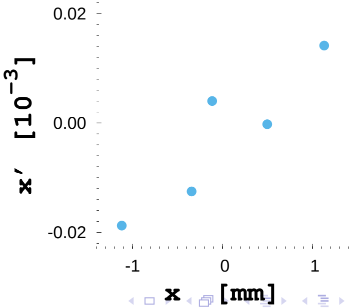

Characterise particle trajectory by position (x) and angle ($x' = \frac{dx}{ds}$)

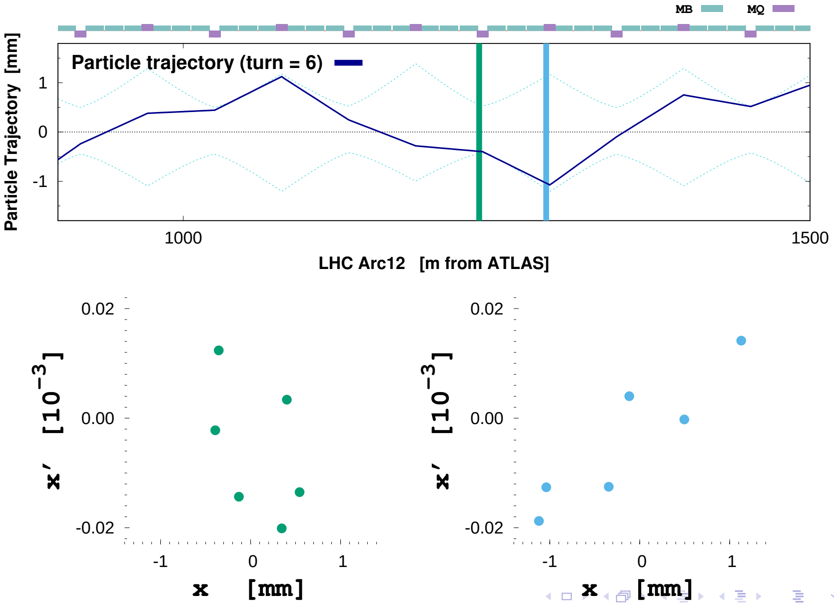

Characterise particle trajectory by position (x) and angle ($x' = \frac{dx}{ds}$)

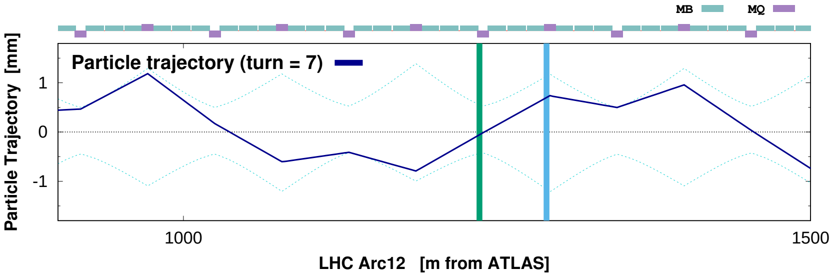

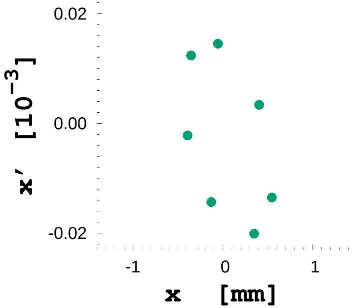

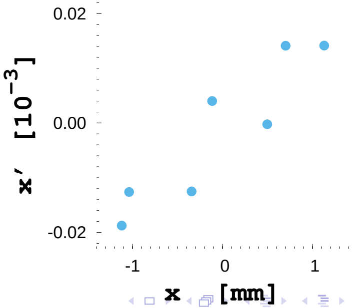

Characterise particle trajectory by position (x) and angle ($x' = \frac{dx}{ds}$)

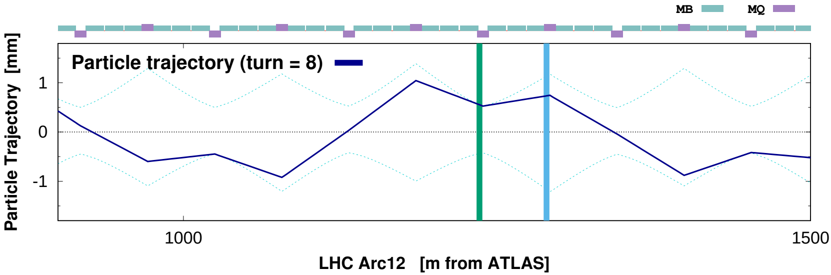

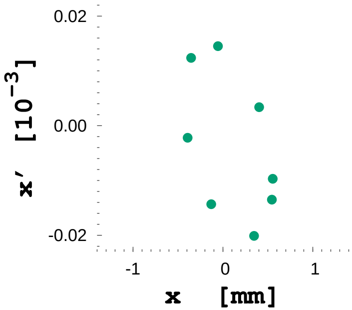

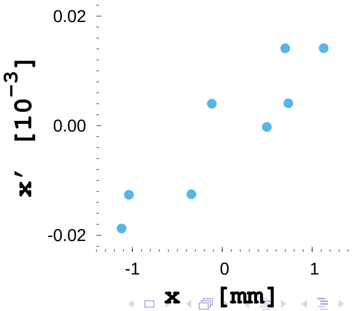

Characterise particle trajectory by position (x) and angle ($x' = \frac{\mathrm{d}x}{\mathrm{d}s}$)

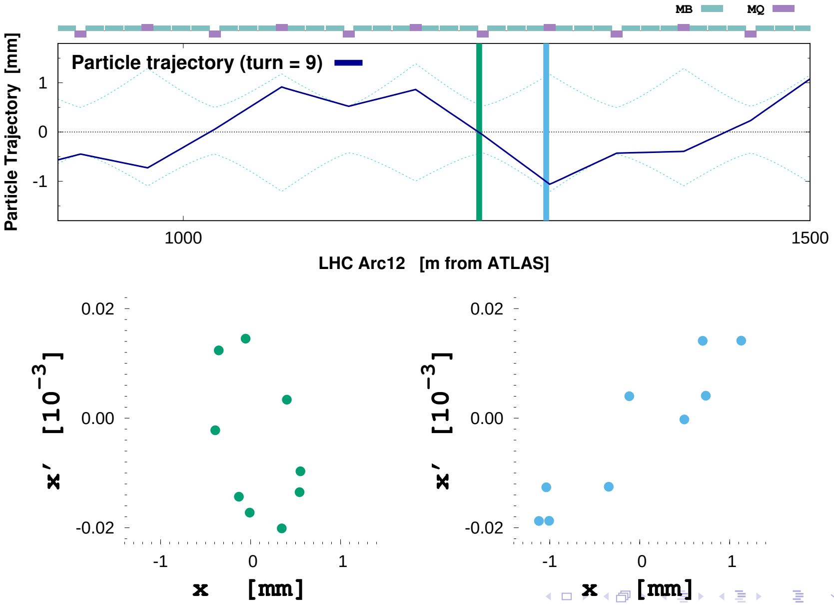

Characterise particle trajectory by position (x) and angle ($x' = \frac{\mathrm{d}x}{\mathrm{d}s}$)

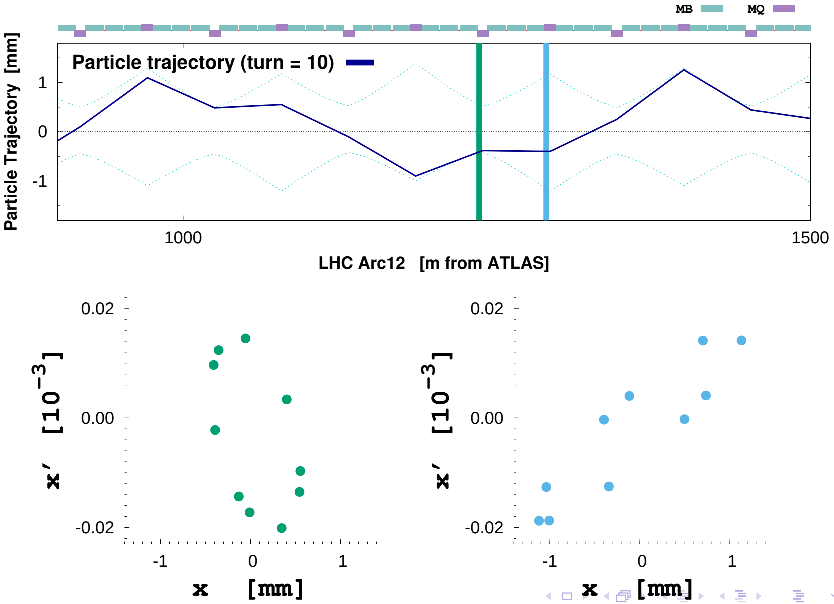

Particles trace out elliptical paths in (x,x') phase space

- '**beam emittance**' is area/π of elipse enclosing 1σ of the particles in the bunch

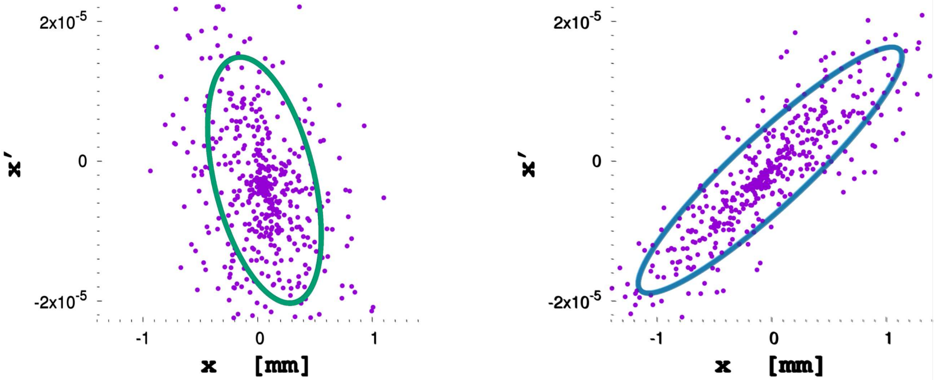

Around 2026-27 LHC will shut down for major upgrades into the High-Luminosity-LHC

- Key component of HL-LHC project is upgrade of LHC injectors e.g. Linac2 (1978) $\rightarrow$ Linac4 (2021)

Around 2026-27 LHC will shut down for major upgrades into the High-Luminosity-LHC

- Key component of HL-LHC project is upgrade of LHC injectors e.g. Linac2 (1978) $\rightarrow$ Linac4 (2021)

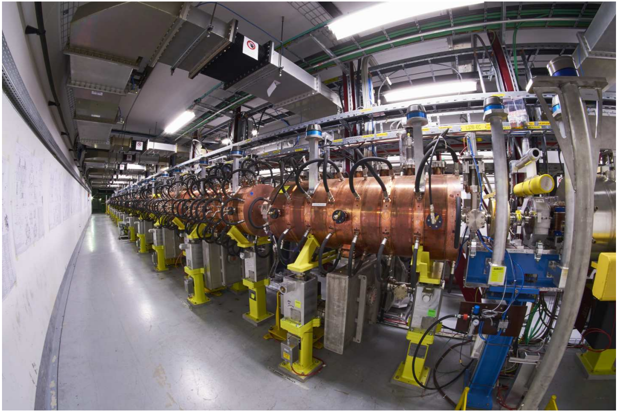

More accurate beam-size description considers coupled 4D-phase-space

$$\Sigma_x^2 = \beta_{11}\epsilon_1 + \beta_{12}\epsilon_2$$
$$\Sigma_y^2 = \beta_{21}\epsilon_1 + \beta_{22}\epsilon_2$$

Betatron motion with coupling of horizontal and vertical degrees of freedom V.A.Lebedev, S.A.Bogacz FERMILAB-PUB-10-383-AD

Plot courtesy T.H.B. Persson (CERN)

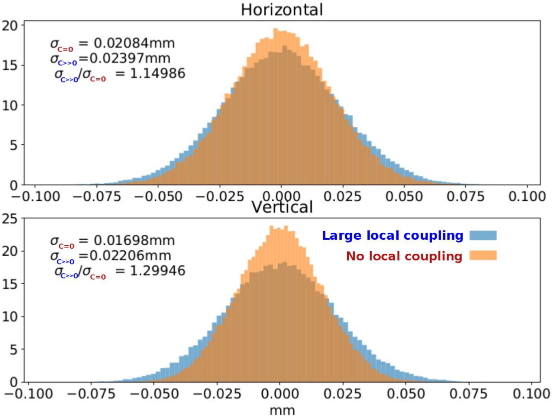

Poor local coupling correction in IR2 during 2018 Pb/Pb run caused 50 % reduction to Luminosity delivered to ALICE until diagnosed & corrected

$$\mathbf{L} = \frac{(f_{rev}\, n_{coll})\ N_1 N_2}{2\pi \sqrt{(\sigma_{x,1}^2 + \sigma_{x,2}^2)} \sqrt{(\sigma_{y,1}^2 + \sigma_{y,2}^2)}}$$

- $N_{1,2}$: **Number of particles per bunch**

- **Beam intensity decays during a fill**
- **Show a corresponding reduction in instantaneous luminosity**
- **Bulk of decay (LHC ideal conditions) is losses of particles which are colliding at the IPs ‘burnoff’**

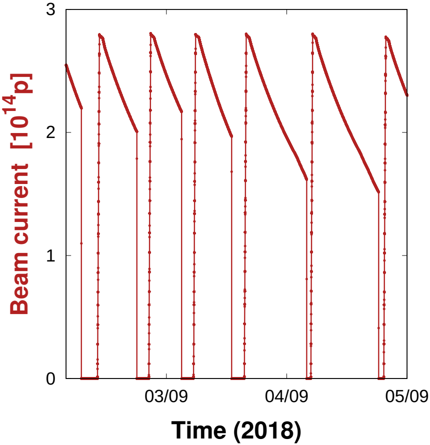

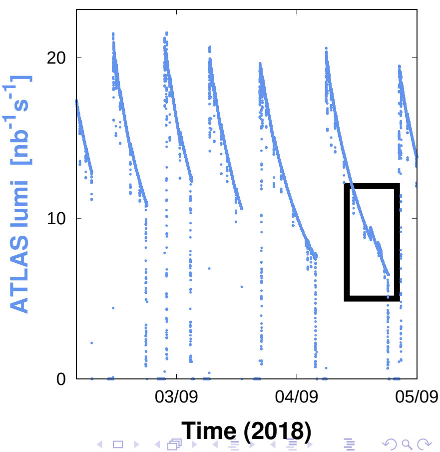

- **Can try to maintain luminosity while $N_{1,2}$ decays by changing other accelerator parameters which influence luminosity**
- '**Luminosity levelling**' $\rightarrow$ e.g. β^*-levelling

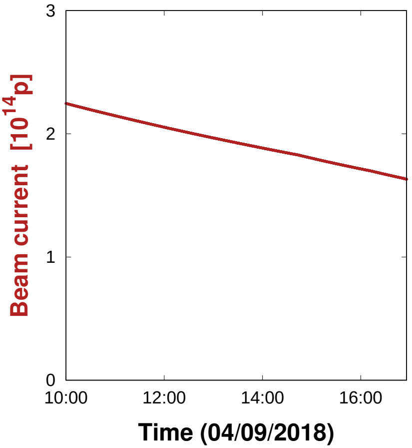

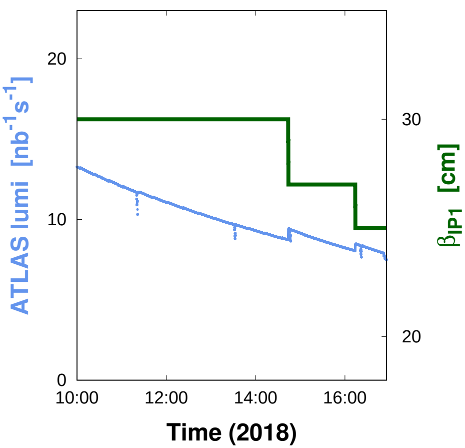

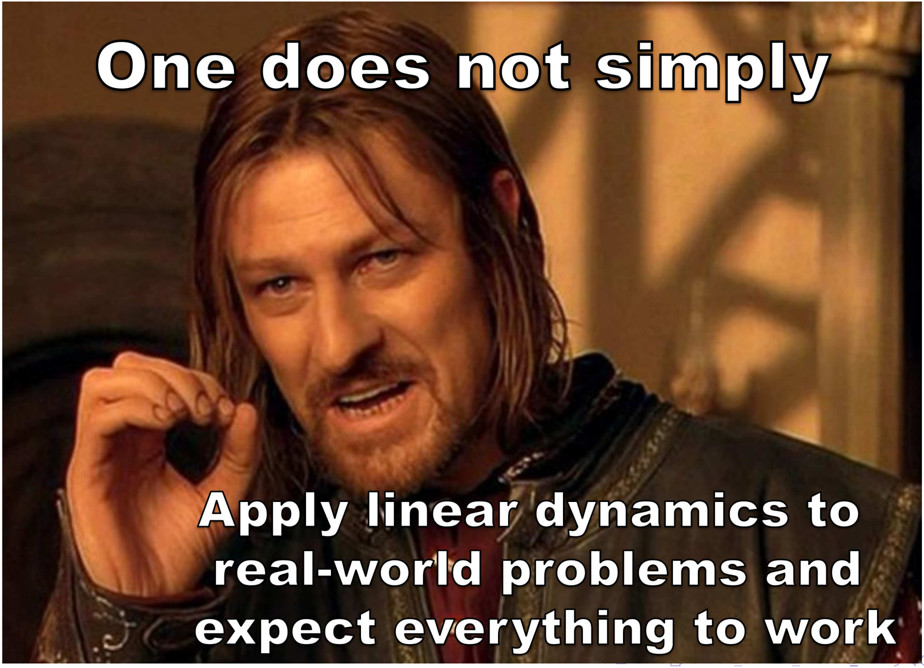
One does not simply
Apply linear dynamics to
real-world problems and
expect everything to work

Large amplitude particles' motion can become chaotic & unstable → '**Dynamic aperture**'

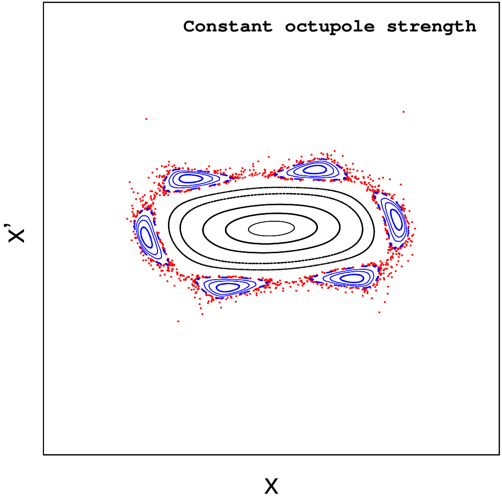

Use sextupole, octupole, decapole & dodecapole magnets to correct nonlinear dynamics in LHC & HL-LHC

The more nonlinear the beam dynamics becomes the smaller the dynamic aperture

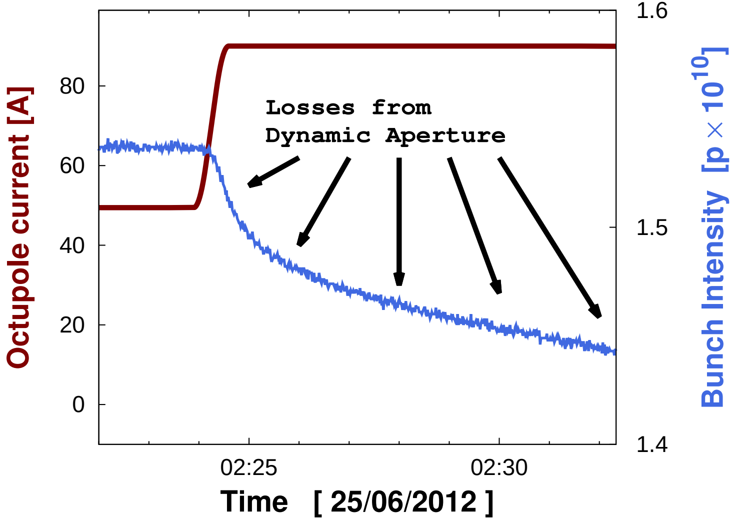

$$\mathbf{L} = \frac{\left(f_{rev}\, n_{coll}\right)\; N_1 N_2}{2\pi\sqrt{\left(\sigma_{x,1}^2 + \sigma_{x,2}^2\right)}\sqrt{\left(\sigma_{y,1}^2 + \sigma_{y,2}^2\right)}}$$

- n_{coll}: **Number of colliding bunches**

How many bunches can we fit in the LHC?

- **LHC revolution frequency** $\approx 11.245\,\mathrm{kHz}$

  $\rightarrow$ **revolution period** $\approx 89\,\mu\mathrm{s}$

- **Minimum separation of bunches defined by RF system of the injector chain**

  $\rightarrow$ **25** ns bunch spacing

soooo... $\approx$ 3560 bunches?

NO!

Also need time to dump / inject beams

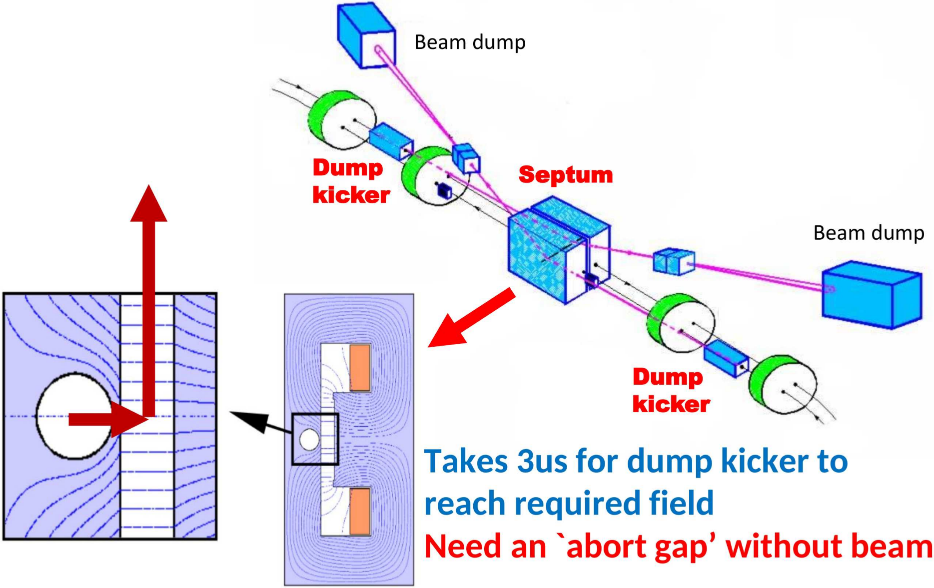

Takes 3us for dump kicker to reach required field

Need an `abort gap' without beam

Also need time to dump / inject beams

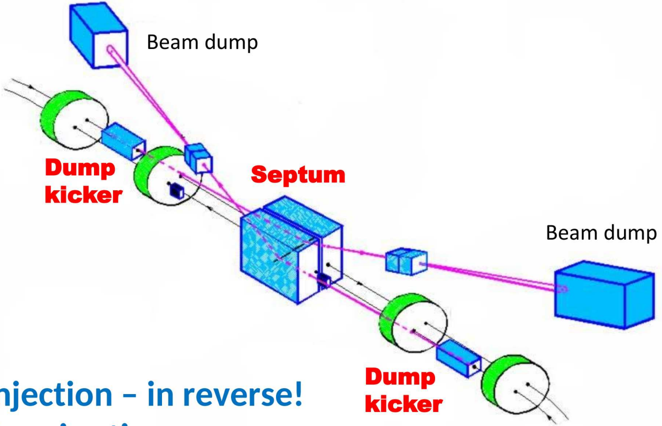

Similar issue at injection – in reverse!
1us injection kicker rise time

Not practical to inject bunches one at a time!

Increase luminosity by colliding trains

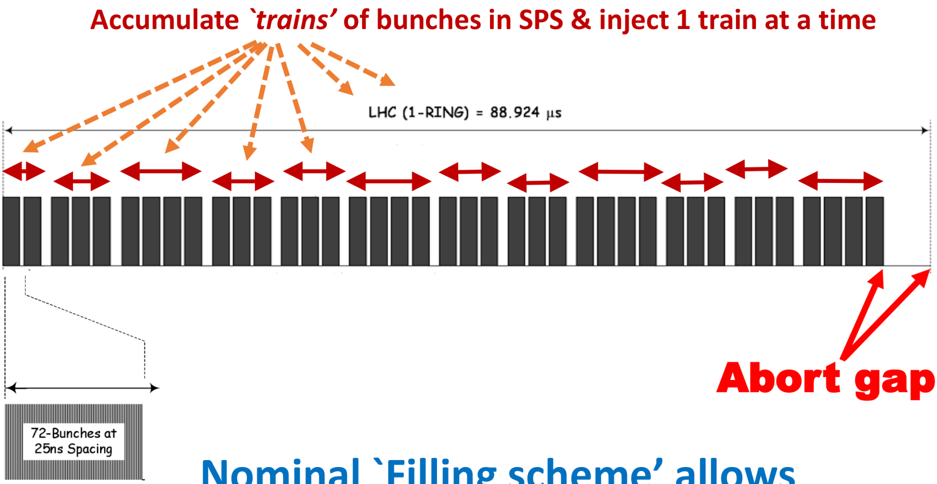

Nominal `Filling scheme' allows 2808 bunches in each ring

In practice many different types of filling scheme are used in the LHC and it may not be desirable to operate with the nominal scheme

Good example of this is `electron cloud'

- seed electron generated by e.g. photoemission / gas ionization
- electron accelerated by field of the beam hits chamber wall
- liberates more secondary electrons
- creates an avalanche of electrons in the beam pipe

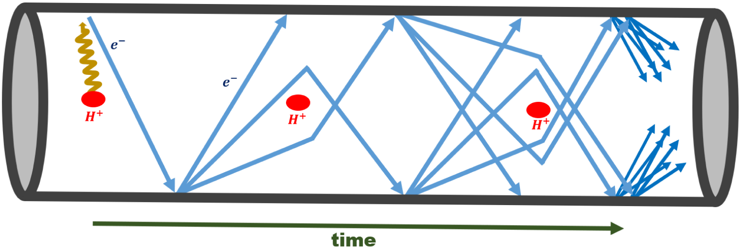

Formation of electron cloud can be suppressed by leaving gaps in the bunch trains:

➡ During parts of Run2 LHC used a special `8b4e' filling scheme (micro-trains of 8 bunches followed by 4 empty slots)

For more details about electron cloud see:
G. Rumolo and G. Iadarola, *Electron Clouds*, CERN Yellow Reports: School Proceedings, Vol. 3/2017, CERN-2017-006-SP
https://doi.org/10.23730/CYRSP-2017-003

Key Points

- **What is luminosity?**
- **What are its main dependencies?**
- **There are many complications which can affect the luminosity!**

Event rate for a HEP interaction:

$$\mathbf{R} = \mathbf{L} \times \boldsymbol{\sigma}$$

- **R:** *Event Rate* $[\mathbf{s^{-1}}]$
- **σ:** *Cross Section* $[\mathbf{barn} = \mathbf{10^{-34} cm^2}]$
  property of the HEP interaction
- **L:** *Luminosity* **[inverse barn / s]**
  property of the collider

Total number of interactions defined by the Integrated Luminosity [inverse femto-barn]

$$\mathbf{N} = \left(\int \mathbf{L(t)dt} \right) \times \boldsymbol{\sigma}$$

Integrated Luminosity is key figure of merit for collider like LHC

$\rightarrow$ significant factor is how much time spent on luminosity production

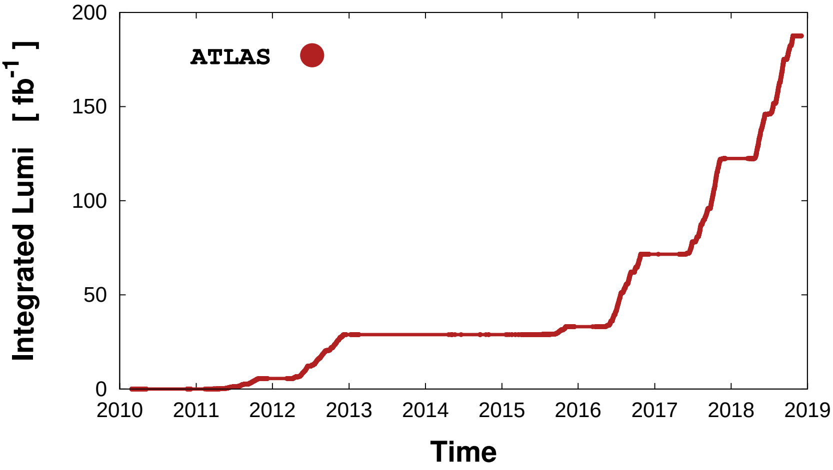

https://lhc-statistics.web.cern.ch/LHC-Statistics/

Approximate schedule for LHC lifetime (accurate up to 2023)

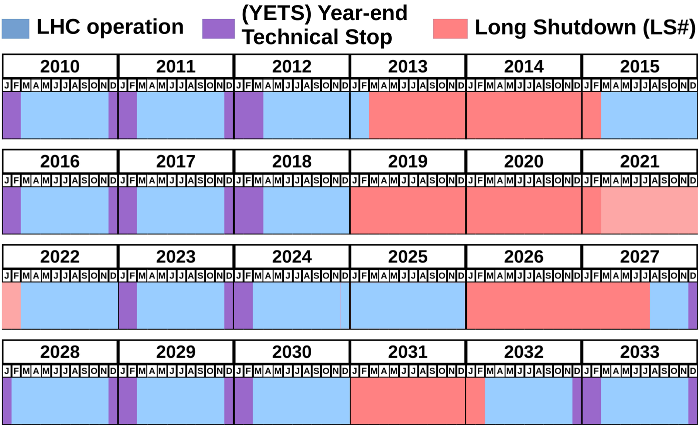

- LHC operation is interspersed with regular **shutdown** periods for maintenance and upgrades

LHC schedule over 1 year (2017)

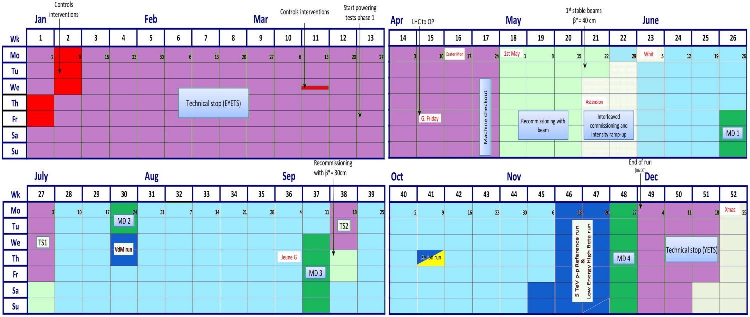

Many types of activities during 1 year of LHC operation

- **Technical Stop (YETS + regular breaks)**
- **Accelerator commissioning**
- **Accelerator physics/technology studies**
- **Luminosity production proton-proton and special runs**

Turn-around-time between stable-beams is a key factor in achieved integrated luminosity!

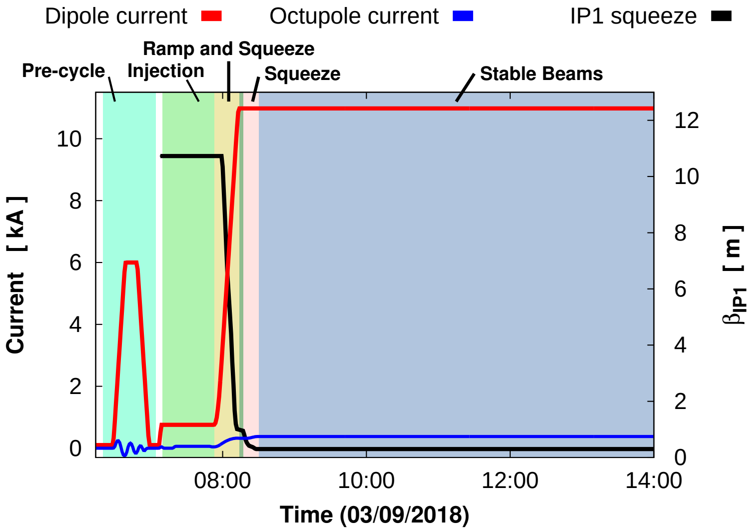

Key Points

- **Integrated luminosity is the key figure of merit for a collider like the LHC**
- **How much time is actually spent colliding beams together?**
- **What are we doing the rest of the time?**

The Future of laboratory based HEP?

$$\Delta E/\mathrm{turn} \propto \frac{(\beta_{rel}\gamma_{rel})^4}{\rho}$$

$$B\rho \ \ [\mathrm{Tm}] = \frac{10}{2.998}\, p \ \ [GeV/c]$$

- **linear e/e colliders (ILC/CLIC)**
- $100\,\mathrm{km}$ **e/e collider ring (FCC-ee,CEPC)**
- **New magnets in LHC tunnel (HE-LHC)**
- $100\,\mathrm{km}$ **hadron collider (FCC-hh,SppC)**

Lots of interest to accelerate/collide new types of particles!

- Substantial R&D ongoing into next-gen Muon collider
- Not limited by synchrotron radiation
- Advantage of colliding elementary leptons vs composite protons
- Very significant challenge to produce/cool/accelerate muons before they decay!

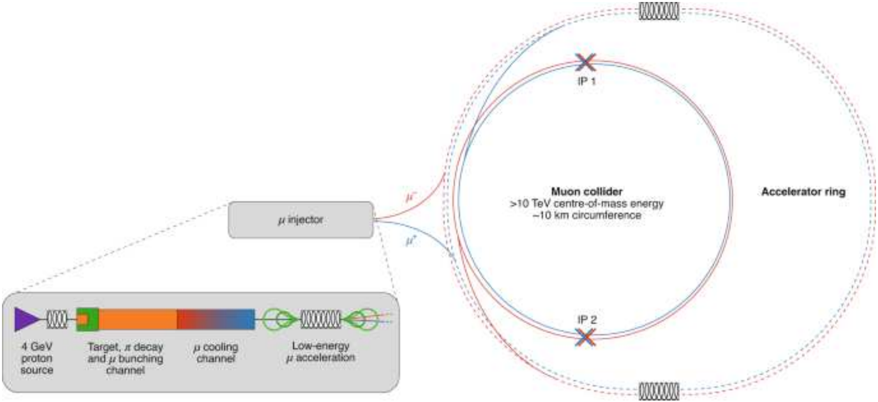

Lots of interest to accelerate/collide new types of particles!

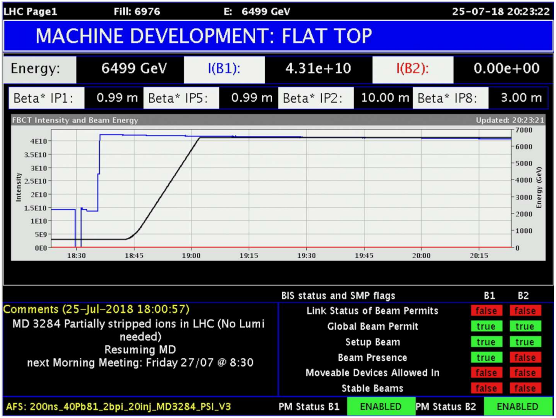

- **Collide with photons!**
- **In 2018 LHC accelerated Pb^{81+} to study potential future use of LHC as a γ-factory**
- **Various ideas of how to use accelerators e.g. CLIC as γ/γ colliders**

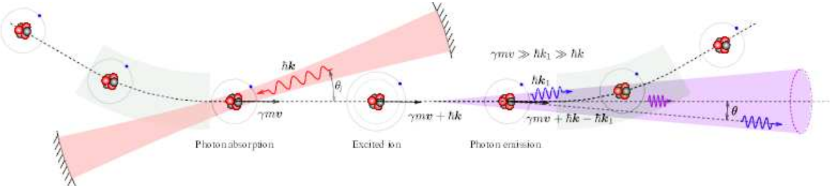

Could future accelerators be used to detect gravitational waves?

- Been considered on/off since ≈1960s
- Some resurgence of interest since discovery by LIGO / proposal of FCC

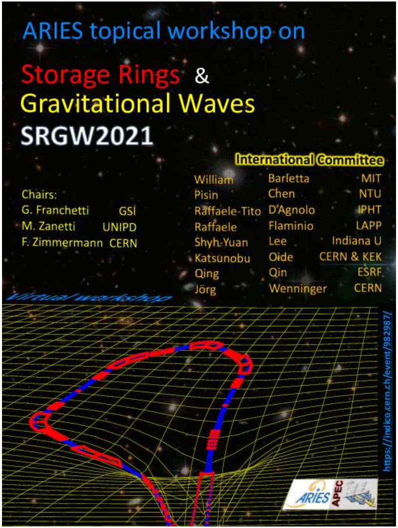

Miniturization of low/intermediate energy accelerators will be one of the key developments of accelerator field for impact on society

- **One of the most exciting topics in accelerator field today is cancer treatment via FLASH therapy with electron beams!**
- **Requires high-quality, high-energy electron beams on a hospital scale**
- **Lots of interest in applying RF technology from CLIC to FLASH!**

Radiotherapy and Oncology 124 (2017) 365–369

Contents lists available at ScienceDirect

Radiotherapy and Oncology

journal homepage: www.thegreenjournal.com

Flash irradiation

Irradiation in a flash: Unique sparing of memory in mice after whole brain irradiation with dose rates above 100 Gy/s

Pierre Montay-Gruel [a,b,1], Kristoffer Petersson [c,1], Maud Jaccard [c], Gaël Boivin [a], Jean-François Germond [c], Benoit Petit [a], Raphaël Doenlen [d], Vincent Favaudon [b], François Bochud [c], Claude Bailat [c], Jean Bourhis [a,1], Marie-Catherine Vozenin [a,*,1]

[a] Department of Radiation Oncology/DO/CHUV, Lausanne University Hospital, Switzerland; [b] Institut Curie, INSERM U1021/CNRS UMR3347, Université Paris-Saclay, Orsay, France; [c] Institute of Radiation Physics (IRA), Lausanne University Hospital; and [d] Faculty of Life Sciences, Ecole Polytechnique Fédérale de Lausanne, Switzerland

ARTICLE INFO

Article history:
Received 27 October 2016
Received in revised form 13 April 2017
Accepted 4 May 2017
Available online 22 May 2017

Keywords:
Flash-RT
Whole brain irradiation
Cognition's preservation

ABSTRACT

This study shows for the first time that normal brain tissue toxicities after WBI can be reduced with increased dose rate. Spatial memory is preserved after WBI with mean dose rates above 100 Gy/s, whereas 10 Gy WBI at a conventional radiotherapy dose rate (0.1 Gy/s) totally impairs spatial memory.

Our recent publications have shown that irradiation at an ultra-high dose rate was able to protect normal tissue from radiation-induced toxicity. When compared to radiotherapy delivered at conventional dose rates (1–4 Gy/min), this so called "Flash" radiotherapy (>40 Gy/s; Flash-RT) was shown to enhance the differential effect between normal tissue and tumor in lung models [1,2] and consequently allowed for dose escalation. The biological interest of Flash-RT seems to rely essentially on a specific, yet undefined, response occurring in normal cells and tissues. We initially hypothesized that the protective effect of Flash was related to the high dose rate delivery, in other words related to the very short time of exposure. In order to further explore Flash-RT and to validate its protective effect on normal tissues, we decided to extend our observation from the lung to other organs. We decided to investigate brain response to Flash-RT as it is a well-defined and robust model in radiobiology [3–5].

When dealing with unexpected biological results, such as the ones previously described with Flash-RT, accurate dosimetry of the delivered irradiation is essential. However, dosimetry at (an ultra-)high dose rate in high dose-per-pulse beams is non-trivial as current radiotherapy dosimetry protocols are not designed for such conditions and because the detectors available for online measurements (i.e. ionization chambers, diodes, and diamond detectors) start to saturate when the dose rate/dose-per-pulse is increased beyond what is used in conventional radiotherapy [6–8]. Therefore, we needed to rely on dosimeters that had been previously validated to function accurately at more extreme irradiation conditions, i.e. mainly passive dosimeters. Among these options, we selected thermo-luminescent dosimeter (TLD) chips because of their small size (3.2 × 3.2 × 0.9 mm^3) so that they could be used for measuring dose in the brain of mice. By positioning the TLD inside the skull of a sacrificed mouse, we were able to validate the dose delivered to the brain during whole brain irradiation (WBI).

Brain injuries after WBI at sub-lethal doses delivered at conventional radiotherapy dose rates are well described [5,9,10]. They include functional alterations, neuronal [11], glial [12,13] and vasculature toxicities [14,15]. Cognitive impairments are the most described functional defects observed in mice and humans following WBI [4,16]. They are caused by an alteration of hippocampal neurogenesis, which can occur as early as one month post 10 Gy single fraction WBI [17]. These cognitive impairments can be evaluated using the "Novel Object Recognition test" [18] on WBI murine models [19]. Therefore, we used this assay to investigate the functional effect of Flash-RT on the normal brain of irradiated mice.

Using a combination of accurate dosimetry measurements and robust biological tests, we first aimed to investigate the potential neuroprotective effect of Flash-RT and indeed found memory preservation in mice after 10 Gy WBI with Flash-RT (delivered in

* Corresponding author at: Laboratoire de Radio-Oncologie, Centre Hospitalier Universitaire Vaudois, Bugnon 46, 1011 Lausanne, Switzerland.
E-mail address: marie-catherine.vozenin@chuv.ch (M.-C. Vozenin).
1 Equal contribution.

http://dx.doi.org/10.1016/j.radonc.2017.05.003
0167-8140/

RESEARCH ARTICLE

RESULTS

FLASH irradiation protects lungs from radiation-induced fibrosis

Two hundred forty mice were divided into groups (n = 5 to 14), sham-irradiated or exposed to single-dose 15- or 17-Gy CONV (^{137}Cs γ-rays) or 17-Gy FLASH (4.5-MeV electrons) through bilateral thorax irradiation, and then sampled at 8, 16, 24, and 36 weeks post-irradiation (pi) for evaluation of complications and histopathological analysis of lung fibrosis.

The initiation and development of pulmonary fibrosis was compared in mice exposed to 17 Gy in either the CONV or FLASH mode (Fig. 1A). Fibrogenesis in the CONV group started as early as 8 weeks pi and progressively worsened, resulting in dense intraparenchymal fibrosis at 24 weeks pi (Fig. 1, A to C). At this time, 4.5-MeV electrons given at the CONV dose rate were as efficient as ^{137}Cs γ-rays with regard to the production of fibrogenic patterns in the lung (Fig. 1A). Pulmonary lesions consisted of consolidated foci, localized mostly in subpleural areas and sometimes at the extremity of pulmonary lobes or in peribronchic areas (Fig. 1A, HES panels, and fig. S9). These foci were characterized as interstitial fibrosis by Masson's trichrome staining (Fig. 1A, MT panels), with thickening and reorganization of alveolar septa, intense collagen deposition, and activation of the transforming growth factor–β (TGF-β)/SMAD cascade (fig. S10) but with few signs of wound healing, scarring, or retraction. Major signs of inflammatory lesions were seen at 24 weeks pi (quantification in fig. S11), with infiltration of alveolar septa by eosinophilic to foamy macrophages, occasional multinucleated giant cells associated with lymphocytes, and plasma cells or occasional neutrophils frequently obliterating residual alveolar lumens. 15-Gy CONV was sufficient to initiate lung fibrosis, as expected (7–10). In contrast, no histological signs of pulmonary fibrosis (Fig. 1, A to C) and no activation of the TGF-β/SMAD4 cascade (fig. S10) were observed in the 17-Gy FLASH group.

A dose escalation study of 16- to 30-Gy FLASH was then performed (n = 52). Mice that had received 20-Gy FLASH did not develop lung fibrosis (Fig. 1C). No macroscopic signs of cutaneous lesions were observed either, although we observed well-delimited hair depigmentation restricted to the irradiated area (Fig. 1D and fig. S11), consistent with the fact that the dose delivered to animals was ≥15 Gy (12). In contrast, animals exposed to 17-Gy CONV developed severe cutaneous lesions within the irradiated field (fig. S11). Mice exposed to ≥23-Gy FLASH experienced cachexia within 32 weeks pi. After 24 weeks pi, 30-Gy FLASH resulted in massive pulmonary edema and fibrotic intraparenchymal patches with inflammatory lesions and macrophage infiltration in thickened alveolar lumens (Fig. 1A). In conclusion, FLASH was shown to be less fibrogenic than CONV irradiation (Fig. 1, A to C).

FLASH protects blood vessels and bronchi from radiation-induced acute apoptosis

Early (1 hour pi) and late (24 hours pi) features of apoptosis were probed in histological sections of irradiated lungs by the determination of caspase-3 cleavage and terminal deoxynucleotidyl transferase (TdT)–mediated deoxyuridine triphosphate (dUTP) nick end labeling (TUNEL) labeling, respectively. 7.5-Gy CONV was sufficient to induce massive cleavage of caspase-3 at 1 hour pi in nuclei from vascular and bronchial smooth muscle cells, whereas no cleaved caspase-3 staining was observed in animals exposed to 17-Gy FLASH (Fig. 2A). In animals exposed to 7.5-Gy CONV, TUNEL-positive nuclei were observed 24 hours pi in epithelial cells of the bronchi, inflammatory cells embedded into the stroma, and smooth muscle cells surrounding the bronchi (Fig. 2B). No TUNEL staining was observed in pulmonary cells of the animals exposed to 17-Gy FLASH, but rare inflammatory cells invading the tissue proved to be TUNEL-positive (Fig. 2B). 30-Gy FLASH was required to induce caspase-3 and TUNEL responses to an extent similar to that of 7.5-Gy CONV.

These observations suggest that vascular apoptosis in the lung could be the primary signal that would trigger long-term complications, including fibrosis, as already suggested in the gut (13). To test this model, 24 hours before radiation, mice were exposed to tumor necrosis factor–α (TNF-α), a key cytokine involved in endothelial cell apoptosis, inflammation, myofibroblast transdifferentiation, and the pathogenesis of radiation pneumonitis (14, 15). Apoptosis was monitored 2 hours pi with the IVIS Spectrum system (PerkinElmer) and a fluorescent annexin V probe for in vivo imaging. In the absence of TNF-α, the total signal of annexin V fluorescence after 30-Gy FLASH was twofold lower than that after 15-Gy CONV (Fig. 2C), thus confirming the low proapoptotic potential of FLASH irradiation. TNF-α alone increased the annexin V signal by 26-fold over nontreated controls. In mice exposed to 15-Gy CONV or 30-Gy FLASH, complementation by TNF-α increased the amount of fluorescence by two- and fourfold, respectively (Fig. 2C). Mice survived these treatments, thus allowing follow-up until 15 weeks pi. At this time, massive edema and fluid extravasation (Fig. 2D, asterisks), which are signs of persistent vascular lesions, were present in the TNF-α–treated groups. Patches of subpleural fibrosis (Fig. 2D, black arrow) were observed only in the group treated with 15-Gy CONV.

In conclusion, TNF-α promoted acute apoptosis in the lungs of FLASH-irradiated animals and triggered dramatic pulmonary edema, consistent with enhanced vascular permeability. However, TNF-α did not induce lung fibrosis in FLASH-irradiated animals within the time range investigated. This observation suggests that protection against vascular apoptosis is only a part of the nonfibrogenic character of FLASH.

FLASH is as efficient as CONV in controlling xenografted human tumors

Human breast cancer HBCx-12A tumor xenografts (fig. S12) were exposed to 17-Gy FLASH or CONV in two equal fractions at a 24-hour interval. FLASH was as efficient as CONV in repressing tumor growth (Fig. 3).

Human head and neck carcinoma HEp-2 xenografts (fig. S12) were then established and exposed to 15-, 20-, or 25-Gy FLASH, or 19.5-Gy eq CONV in a single fraction. After 40 days pi, dose-dependent inhibition of tumor growth was observed in all irradiated groups regardless of the radiation source and dose rate used. Remarkably, 25-Gy FLASH allowed a complete tumor growth arrest after 40 days pi (Fig. 3), without any skin damage in the irradiated area.

FLASH is as efficient as CONV in controlling syngeneic, orthotopic lung tumors

We used a syngeneic, orthotopic tumor model, consisting of TC-1 cells (C57BL/6J mouse lung carcinoma) engineered to express luciferase (TC-1 Luc$^+$) and transpleurally injected into the lung of C57BL/6J mice, to compare normal tissue and tumor responses at the maximum tolerated doses by the lung in each mode, CONV or FLASH, over 9 weeks pi. The evolution of the disease in each mouse was followed by bioluminescence analysis and confirmed by histopathology (Fig. 4, A to C).

Very interesting work storing single particles at IOTA accelerator in US!

Accelerator research

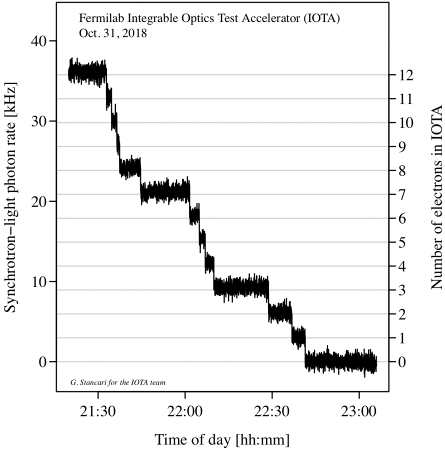

https://news.fnal.gov/2018/11/single-electron-beam-observed-in-iota-for-the-first-time/

10th Int. Particle Accelerator Conf. IPAC2019, Melbourne, Australia JACoW Publishing
ISBN: 978-3-95450-208-0 doi:10.18429/JACoW-IPAC2019-MOPRB089

EXPERIMENTAL STUDY OF A SINGLE ELECTRON IN A STORAGE RING VIA UNDULATOR RADIATION

S. Nagaitsev*,[1], G. Stancari, A. Romanov, Fermilab, Batavia, USA
A. Arodzero, A. Murokh, M. Ruelas, RadiaBeam Technologies, Santa Monica, USA
I. Lobach, The University of Chicago, Chicago, USA
T. Shaftan, BNL, Upton, USA
[1]also at the University of Chicago, Chicago, USA

Abstract

A single electron orbiting around a ring and emitting single quanta at the rate of about one event per hundred turns could produce a wealth of information about physical processes in large traps (i.e. storage rings) for charged particles. It should be noted that Paul and Penning traps in the 1980s led to the Nobel prize for studying state and motion of single quantum particles, and just recently the Penning trap technique has enabled the measurement of a single proton magnetic moment with an unprecedented precision of 10 decimal places. The information from the storage ring traps could also be used for characterization of a quantum system as well as the "trap" itself, i.e. measuring properties of the storage ring lattice and electron interaction with the laser fields. Although, the interest in single electron quantum processes today is mostly academic in nature, the diagnostics and methodology developed for single electron radiation studies could find subsequent applications in a variety of applied disciplines in quantum technology, including quantum communications and quantum computing.

INTRODUCTION

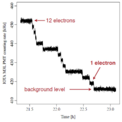

Figure 2: A measured photo-multiplier signal from a synchrotron radiation monitor after the bend magnet. One can clearly see finite jumps in the average proton count rate level as the number of trapped electrons becomes small, until a single electron is left in the IOTA storage ring.

PHYSICAL REVIEW ACCELERATORS AND BEAMS **23,** 054701 (2020)

Towards storage rings as quantum computers

K. A. Brown* and T. Roser
Brookhaven National Laboratory, Upton, New York 11973-5000, USA

(Received 28 February 2020; accepted 4 May 2020; published 13 May 2020)

We explore the possible use of particle beam storage rings as quantum computers. More precisely, we consider creating an ion trap system, in which the same computational basis states can be defined as in a modern ion trap system, but in which the ions have a constant velocity and are rotating in a circular trap. The basic structures that we explore are classical and ultracold crystalline beams. What we propose is a novel method that uses the ion trap quantum computer concept, but puts the ions into a rotating frame of reference. The benefits of this approach are discussed.

DOI: 10.1103/PhysRevAccelBeams.23.054701

I. INTRODUCTION

A particle accelerator storage ring is an apparatus that stores charged particle beams. The beams, if not cooled, can have very high temperatures and can be treated as classical thermodynamic ensembles of particles confined to some volume. When stored, either as bunches of particles or debunched into a uniform longitudinal (temporal) distribution, the ensemble is in steady state and has constant entropy. In general, such a beam has no specific structure and should act like an ideal gas. However, the particles are necessarily charged and can interact with each other through intrabeam collisions and other phenomena. These processes can cause beam heating, increasing the entropy. In addition, these particle distributions do contain information encoded into the behavior of the beams as they traverse the electromagnetic optics that keep them confined within the storage ring [1–4].

$$\epsilon_u = 4\pi(\langle u^2\rangle\langle u'^2\rangle - \langle uu'\rangle^2)^{\frac{1}{2}}, \quad (1)$$

where c_u is the horizonal or vertical beam emittance. We will call the transverse beam temperature the temperature associated with the transverse emittance. Longitudinally, the temperature, T, is a function of the momentum spread [8],

$$\frac{1}{2}k_B T = \frac{1}{2}m(\delta v)^2, \quad (2)$$

where δv is the spread in velocity of the ions in the beam. k_B is Boltzmann's constant. In more practical units, temperatures for ion beams can be expressed as,

$$T_{\|}[K] = \frac{2}{k_B}\left(\frac{\delta p}{p_0}\right)E_0[\text{eV}] \quad (3)$$

Many thanks for your attention!